European Journal of Medicinal Chemistry 208 (2020) 112789

Contents lists available at ScienceDirect

European Journal of Medicinal Chemistry

journal homepage: http://www.elsevier.com/locate/ejmech

Synthesis and in vitro and in vivo biological evaluation of novel derivatives of flexicaulin A as antiproliferative agents

Jun-Feng Huo [a, b], Tian-Xing Hu [a, b], Ya-Long Dong [a, b], Jin-Zhu Zhao [a, b], Xiao-Jie Liu [a, b], Lei-Lei Li [a, b], Xue-Yan Zhang [a, b], Yun-Fan Li [a, b], Hong-Min Liu [a, b, **], Yu Ke [a, b, ***], Cong Wang [a, b, *]

[a] State Key Laboratory of Esophageal Cancer Prevention & Treatment, School of Pharmaceutical Sciences, Zhengzhou University, Zhengzhou, Henan Province, 450001, PR China
[b] Key Laboratory of Advanced Drug Preparation Technologies, Ministry of Education of China, Zhengzhou University, Zhengzhou, Henan, 450001, PR China

ARTICLE INFO

Article history:
Received 14 June 2020
Received in revised form
25 August 2020
Accepted 25 August 2020
Available online 31 August 2020

Keywords:
Isodon plants
Ent-kaurene diterpene
Antiproliferative activity
ROS/JNK pathway

ABSTRACT

As our research focuses on anticancer drugs, a series of novel derivatives of flexicaulin A (FA), an *ent*-kaurene diterpene, condensed with an aromatic ring were synthesized, and their antiproliferative activities against four human cancer cell lines (TE-1, EC109, MCF-7, and MGC-803) were evaluated. The activities of most of the new compounds were better than those of FA. Compound **2y** exhibited the best activity with an IC50 value reaching 0.13 μM against oesophageal cancer cells (EC109 cells). The IC50 values for **2y** in normal cells (GES-1 cells and HUVECs) were 0.52 μM and 0.49 μM, respectively. Subsequent mechanistic investigations found that compound 2y can inhibit the proliferation of cancer cells and cell cloning. In addition, **2y** could reduce the mitochondrial membrane potential, increase the apoptosis rate, and increase the ROS level in EC109 cells. Moreover, 2y can upregulate the expression of ROS/JNK pathway-related proteins (p-ASK1, p-MKK4, p-JNK, and p-Cjun (ser63)) and pro-apoptotic proteins (Bax, Bad, and Bim). In vivo experiments showed that 2y can inhibit tumour growth in nude mice. The mechanism involves an increase in protein expression in the ROS pathway, leading to changes in apoptosis-related proteins. In addition, compound 2y shows low toxicity. These results indicate that compound 2y holds promising potential as an antiproliferative agent.

1. Introduction

Cancer is the second leading cause of death globally, but there are no drugs that can cure cancer. Therefore, it is urgent to develop anticancer drugs with novel skeletons and mechanisms of action.

Due to its remarkable structural specificity and biological characteristics, natural products [1–3] have always been an essential source of new drugs, especially anticancer drugs. *Isodon* species [4,5] are widely distributed plants, and thus far, more than 600 diterpenoids have been isolated from these species [6–8]. Some of these diterpenoids have shown impressive anticancer activity and low toxicity, especially *ent*-kaurane diterpenes with α,β-unsaturated ketone structures, such as oridonin [9–16], longikaurin A [17], phyllostachysin F, and Jiyuan Oridonin A [18–20] (Fig. 1). There is increasing evidence that the anticancer activity of these diterpenes is induced by inhibiting cell proliferation and inducing apoptosis [15,21–23]. Their impressive structural skeleton promises safe and efficacious profiles for cancer treatment, making them promising anticancer agents.

However, the development of *ent*-kaurene diterpenoids for cancer therapy has been mostly obstructed by their relatively moderate activity, structural complexity, and unclear mechanism of action [14]. Therefore, we urgently need to develop novel diterpenoid derivatives to improve their potency and anticancer activity profile. Previous structure-activity relationship (SAR) studies have

* Corresponding author. State Key Laboratory of Esophageal Cancer Prevention & Treatment; School of Pharmaceutical Sciences, Zhengzhou University, Zhengzhou, Henan Province, 450001, PR China.
** Corresponding author. State Key Laboratory of Esophageal Cancer Prevention & Treatment; School of Pharmaceutical Sciences, Zhengzhou University, Zhengzhou, Henan Province, 450001, PR China.
*** Corresponding author. State Key Laboratory of Esophageal Cancer Prevention & Treatment; School of Pharmaceutical Sciences, Zhengzhou University, Zhengzhou, Henan Province, 450001, PR China.
E-mail addresses: liuhm@zzu.edu.cn (H.-M. Liu), ky@zzu.edu.cn (Y. Ke), wangcong@zzu.edu.cn (C. Wang).

https://doi.org/10.1016/j.ejmech.2020.112789
0223-5234/

revealed that modification of the A ring [24] and 14-hydroxy group of oridonin could significantly increase antiproliferative efficacy [13,25]. For instance, *S. Xu* reported that their most potent compound, which acylates the O-14 position of oridonin with an aromatic ring, was 200-fold more efficacious than oridonin in MCF-7 cancer cells [14].

Flexicaulin A [26–28] (Flexicaulin A, Fig. 1) was first found by H. D. Sun [29]. We successfully extracted FA from Jiyuan *Isodon rubescens* (Donglingcao in Chinese) for the first time. It was interesting and exciting to find a considerable content of FA in Jiyuan *Isodon rubescens*. The weight content of FA in this plant is approximately 1%. In addition, its antiproliferative activity was better than oridonin in various human cancer lines, such as MCF-7 and MGC-803. Moreover, in our previous research, we found that 14 hydroxyl acylation of FA with aromatic ring amino acids could significantly enhance its anticancer activity [28]. In this study, we planned to introduce aromatic ring groups at the O-14 position of FA. To our delight, most of the synthesized compounds displayed better activity than FA against all cancer cell lines selected. Moreover, the anticancer mechanisms of our compounds involved the ROS/JNK signalling pathway. The results reveal the potential of this new diterpenoid as a novel anticancer drug agent.

2. Results and discussion

2.1. Chemistry

The synthetic route of the target FA analogues **2a-2z** is depicted in Scheme 1. Compound 1 was mixed with bromobutyric acid, phenylpropionic acid or different benzoic acids in anhydrous dichloromethane (DCM) and then the reaction was catalysed by 1-(3-(dimethylaminopropyl)-3-ethylcarbodiimide hydrochloride (EDCI) and 4-dimethylaminopyridine (DMAP) to afford compounds **2a-2z** in good yield. All synthesized compounds were characterized by ^{1}H NMR, ^{13}C NMR, and HRMS.

2.2. Biology

2.2.1. In vitro antiproliferative activity and SAR study

The newly synthesized diterpenoid FA derivatives were tested for their antiproliferative activities against four human cancer cell lines, including the EC109 (human oesophageal cancer), TE-1 (human oesophageal cancer), MGC-803 (human stomach cancer) and MCF-7 (human breast cancer) cell lines, and compared with the activity of lead compound FA (1) and positive control oridonin. The cytotoxic activity of the target compounds was detected by SRB assay. The IC_{50} values (concentration required to inhibit cancer cell proliferation by 50%) are listed in Table 1.

From the screening results in Table 1, it was observed that most of the synthesized compounds (compounds **2a**-**2z**) showed enhanced antiproliferative activities compared to FA and oridonin against all four selected cancer lines. The above results demonstrated that the aromatic ring could significantly improve the antiproliferative activity of FA. It was speculated that the lipophilicity of the aromatic groups may enhance the ability of the compounds to cross the cell membrane. Additionally, the position and type of substituent on the aromatic ring had little effect on the anticancer activity. Moreover, modification of the 14 hydroxyl group of FA could improve its antiproliferative activity. The results above would be helpful to research structural modifications of FA.

Among all compounds, compound **2y** exhibited the strongest inhibitory effects against the EC109 (human oesophageal cancer)

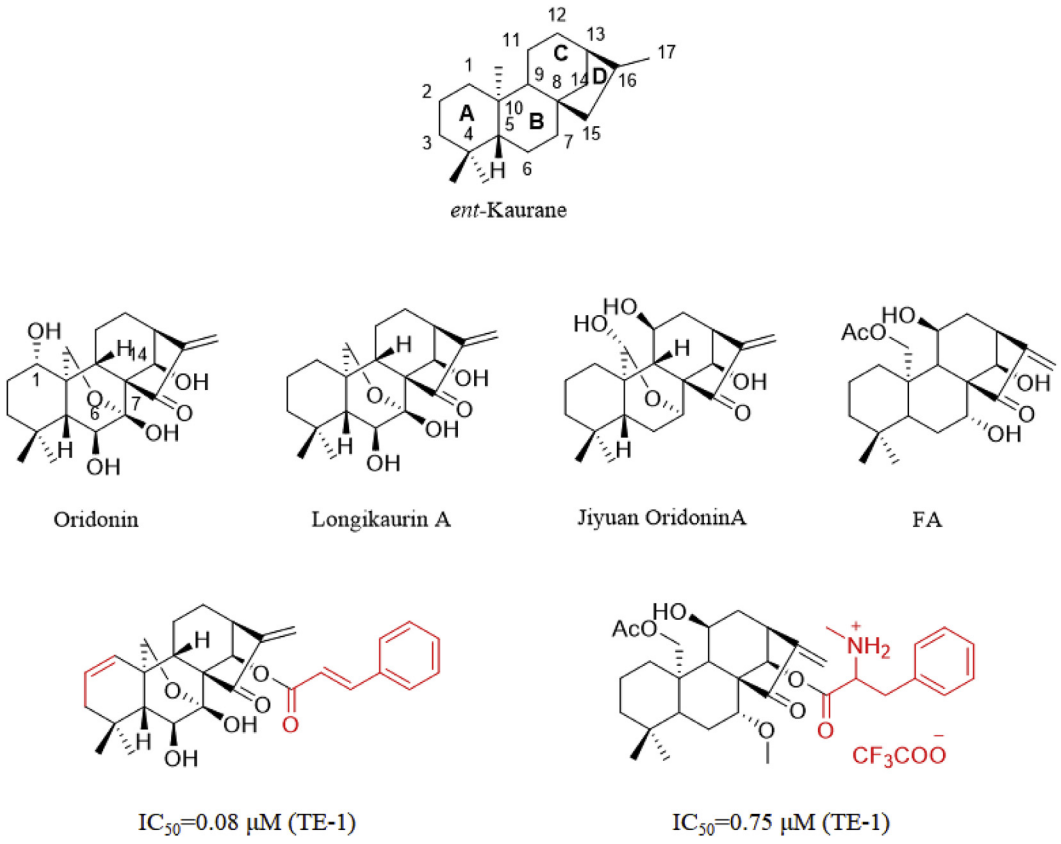

Fig. 1. Structures of *ent*-kaurene diterpenoids from *Isodon* and some representative Oridonin and Flexicaulin A, incorporated with aromatic ring, derivatives have been reported.

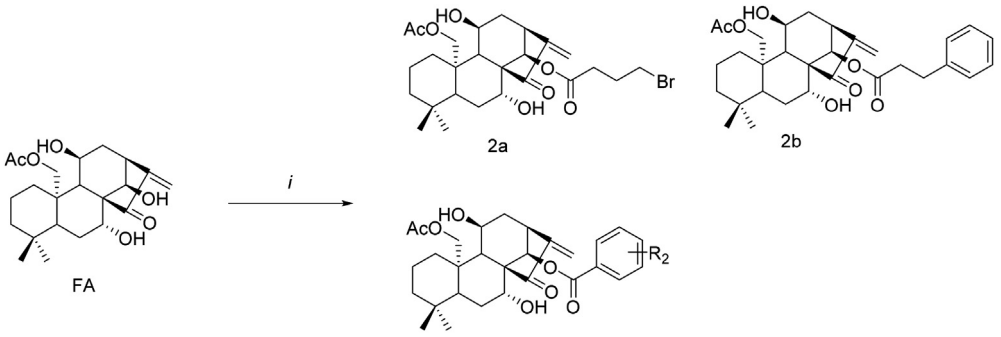

2c R_2=H
2d R_2=2-F-
2e R_2=2-Cl-
2f R_2=2-Br-
2g R_2=2-CH_3-
2h R_2=2-CF_3-
2i R_2=2,3-2Cl-
2j R_2=2,4-2Cl-
2k R_2=2-CH_3O-5-Cl-
2l R_2=3-F-
2m R_2=3-Cl-
2n R_2=3-Br-
2o R_2=3-CH_3O-
2p R_2=3-CH_3-
2q R_2=3-CF_3-
2r R_2=3,4-2CH_3O-
2s R_2=4-F-
2t R_2=4-Cl-
2u R_2=4-Br-
2v R_2=4-CH_3O-
2w R_2=4-CH_3-
2x R_2=4-CF_3-
2y R_2=4-Cl-CH_2-
2z R_2=4-Br-CH_2-

Scheme 1. Synthetic route of series 1. Reagents and conditions: *i*) Bromobutyric acid or Phenylpropionic acid or different benzoic acids, DCM, DMAP/DCC, rt, 4–6h.

Table 1
Inhibitory activities of compounds **2a-2z** against the tested cancer cell lines.

Compound	IC_{50}(μM)			
	EC109	TE-1	MGC-803	MCF-7
FA	5.24 ± 0.92	6.82 ± 0.72	8.70 ± 0.87	6.79 ± 0.66
Oridonin	21.97 ± 1.01	12.73 ± 0.32	14.13 ± 0.51	21.97 ± 1.01
2a	0.76 ± 0.07	0.47 ± 0.04	0.25 ± 0.01	0.47 ± 0.03
2b	0.68 ± 0.04	0.72 ± 0.07	1.28 ± 0.15	0.60 ± 0.02
2c	0.31 ± 0.06	0.33 ± 0.11	0.47 ± 0.03	0.20 ± 0.00
2d	1.63 ± 0.18	3.63 ± 0.42	2.29 ± 0.16	1.72 ± 0.10
2e	0.41 ± 0.03	0.45 ± 0.02	0.71 ± 0.09	0.41 ± 0.01
2f	0.51 ± 0.04	0.37 ± 0.03	0.52 ± 0.08	0.46 ± 0.01
2g	0.47 ± 0.05	0.45 ± 0.02	0.63 ± 0.10	0.39 ± 0.01
2h	0.42 ± 0.04	0.32 ± 0.03	0.79 ± 0.07	0.40 ± 0.03
2i	0.33 ± 0.08	0.39 ± 0.14	0.69 ± 0.07	0.31 ± 0.02
2j	4.25 ± 0.39	1.24 ± 0.12	1.15 ± 0.07	1.17 ± 0.07
2k	0.56 ± 0.05	0.46 ± 0.04	0.66 ± 0.10	0.48 ± 0.01
2l	1.63 ± 0.19	1.30 ± 0.18	2.35 ± 0.19	2.23 ± 0.18
2 m	0.40 ± 0.03	0.41 ± 0.03	0.41 ± 0.06	0.36 ± 0.01
2n	0.24 ± 0.05	0.16 ± 0.04	0.42 ± 0.02	0.38 ± 0.01
2°	0.44 ± 0.02	0.42 ± 0.05	0.46 ± 0.05	0.25 ± 0.03
2p	0.37 ± 0.05	0.32 ± 0.03	0.31 ± 0.04	0.29 ± 0.01
2q	0.33 ± 0.04	0.37 ± 0.03	1.15 ± 0.48	0.29 ± 0.02
2r	0.27 ± 0.06	0.34 ± 0.09	0.57 ± 0.06	0.14 ± 0.01
2s	8.48 ± 0.84	20.07 ± 1.85	0.92 ± 0.05	1.34 ± 0.12
2t	0.33 ± 0.04	0.38 ± 0.03	0.28 ± 0.07	0.27 ± 0.01
2u	0.38 ± 0.03	0.39 ± 0.02	0.61 ± 0.09	0.33 ± 0.01
2v	0.29 ± 0.04	0.25 ± 0.02	0.46 ± 0.05	0.23 ± 0.01
2w	0.30 ± 0.03	0.30 ± 0.03	0.48 ± 0.05	0.24 ± 0.01
2x	0.38 ± 0.03	0.42 ± 0.03	0.77 ± 0.07	0.35 ± 0.02
2y	0.13 ± 0.01	0.27 ± 0.02	0.20 ± 0.01	0.35 ± 0.03
2z	0.17 ± 0.02	0.25 ± 0.02	0.34 ± 0.04	0.14 ± 0.00

[a] SRB methods, cell lines were treated with target compounds for 72h.The average value of the three independent experiments was expressed by mean ± SDs.

and MGC-803 (human stomach cancer) cell lines with IC_{50} values of 0.13 ± 0.01 and 0.20 ± 0.01 μM, respectively. In addition, in the TE-1 (human oesophageal cancer) and MCF-7 (human breast cancer) cell lines, **2y** displayed equivalent activity to the other derivatives. For the above reasons, compound **2y** was chosen for further investigation regarding its mechanism of action against EC109 cells.

2.2.2. The effects of compound **2y** on EC109 cells

First, SRB methods were used to evaluate the antiproliferative effects of compound **2y** towards EC109 cells. As shown in Fig. 2, the survival rate of the cells (EC109, GES-1, and HUVECs) decreased with increasing drug concentrations ranging from 0 to 8 μM and extended time (24, 48, and 72 h). Simultaneously, the 72-h IC_{50} of GES-1 (0.52 μM ± 0.01) and HUVECs (0.49 μM ± 0.03) is higher than EC109 (0.13 μM ± 0.01), which shows that the drug is selective. However, further experiments still need to be explored in vivo. The results revealed that compound **2y** could inhibit cell proliferation in a dose- and time-dependent manner.

To further explore the effects of **2y** on the proliferation of single cells, a clone formation experiment was used to examine the impact of this compound on EC109 cells. As shown in Fig. 2, each dosing group inhibited the cloning ability of EC109 cells. The experimental results show that **2y** can inhibit clone formation of EC109 cells in vitro.

2.2.3. Detection of apoptosis by flow cytometry

The above experiments show that **2y** has significant effects on the proliferation and cloning ability of EC109 cells. An Annexin V-FITC/PI kit was used to further detect the effects of **2y** on EC109 cell apoptosis. As shown in Fig. 3, EC109 cells were treated with **2y** at concentrations of 0.75 μM, 1.5 μM, and 3 μM for 24 h and 48 h, and we obtained the apoptotic rates from each group. The results demonstrated that **2y** could cause apoptosis in EC109 cells in a time-dependent manner.

2.2.4. Effects of compound **2y** on mitochondrial membrane potential in EC109 cells

Previous experiments found that **2y** can induce apoptosis in EC109 cells. However, the way in which this compound affects cell apoptosis needs further study. Mitochondrial membrane potential (MMP) is closely related to apoptosis and it can be detected with JC-1 fluorescent probe [30,31]. In our study, each sample was detected by flow cytometry after EC109 cells were treated with **2y** for 24 h. It can be seen from Fig. 4 that **2y** can induce the mitochondrial depolarization in EC109 cells (red fluorescence shifts to green

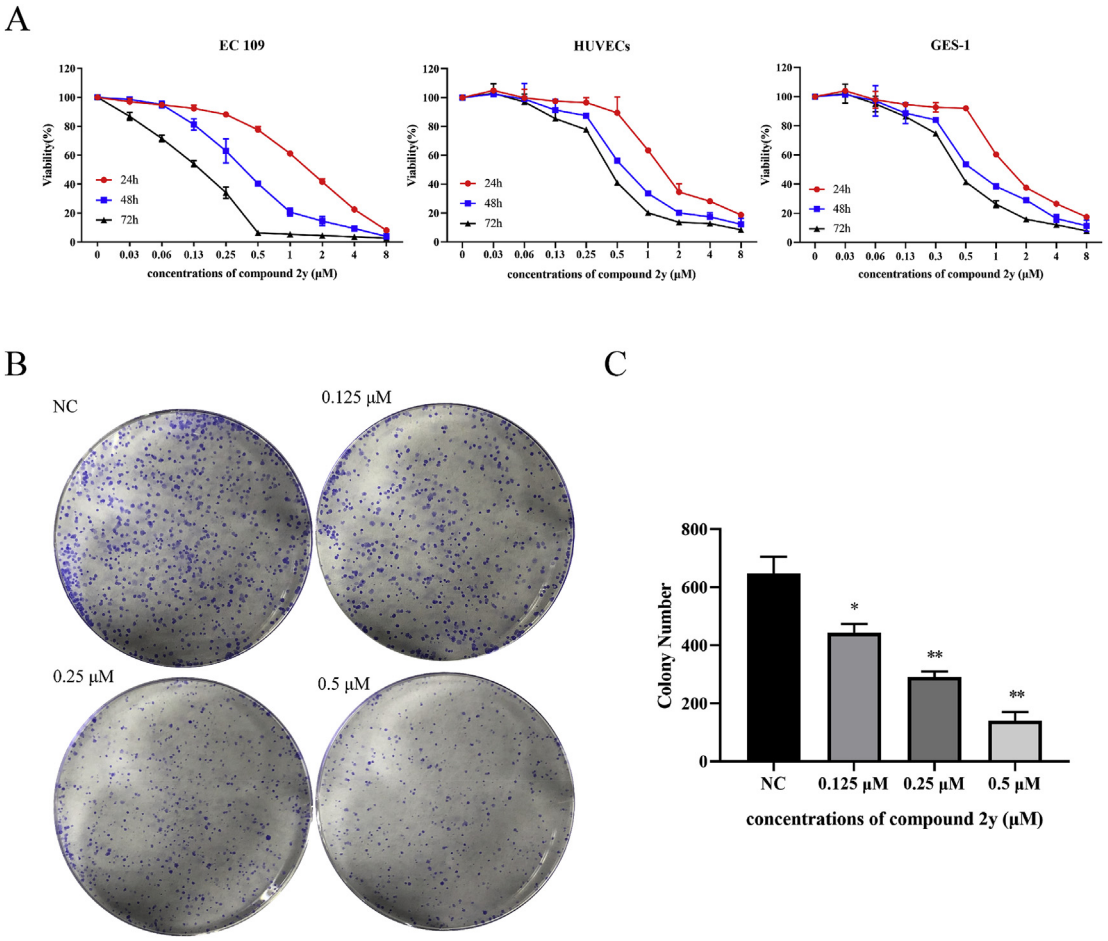

Fig. 2. (A) The effect of compound **2y** in EC109, GES-1, and HUVECs. (B) The colony formation of EC109 cells after treatment with compound **2y** for 7 days. (C) The number of colonies in various drug concentrations. The results shown were representative of three independent experiments. *$p < 0.05$, **$p < 0.01$ verse control.

fluorescence). Moreover, the mitochondrial membrane potential changed significantly at concentrations of 0.75 μM, 1.5 μM and 3 μM. The experimental results suggest that **2y** may induce programmed apoptosis via endogenous mitochondrial damage.

2.2.5. *Effects of compound **2y** on apoptosis-related proteins*

To explore the specific molecular mechanism of the effects of **2y** on apoptosis, we used Western blotting to detect changes in apoptosis-related proteins in EC109 cells after 24 h of drug stimulation. It can be seen from Fig. 5 that the expressions of Cleaved caspase 9, Cleaved caspase 3, Cleaved caspase 7, and Cleaved PARP all increased with increasing drug concentration. This phenomenon occurs because the upstream signalling pathway allows Cleaved caspase 9 to initiate the action of other caspase members, including caspase 3 and caspase 7, to launch the caspase cascade, which in turn leads to apoptosis. Moreover, cleaved caspase 3 can further Cleave PARP.

The caspase cascade leads to apoptosis and is initiated by cleavage of caspase 9. There is substantial literature that shows that the cleavage of caspase 9 could lead to apoptosis [32,33]. According to the above mitochondrial membrane potential experiment, Western blotting was used to detect Bcl-2 family-related proteins (Fig. 5). The results showed decreased expression of the anti-apoptotic protein Bcl-2 and increased expression of the pro-apoptotic proteins Bad and Bim (Bim_{EL}, Bim_L, and Bim_S) with increasing drug concentration, but the expression of Bax did not change significantly. However, the ratio of Bax/Bcl-2 increased. The increased expression of Bad and Bim can lead to a decline in anti-apoptotic proteins in the Bcl-2 family, which is consistent with the results of the above-mentioned Bcl-2 protein reduction [34,35]. Finally, we found that the expression of cytochrome C increased with increasing drug concentration. The above experiment shows that **2y** activates the pro-apoptotic proteins Bim and Bad, which causes decreased expression of the anti-apoptotic protein Bcl-2. This simultaneously leads to an increase in the ratio of Bax/Bcl-2 to release cytochrome C, which causes cytochrome C to Cleave caspase 9. Finally, the caspase cascade leads to apoptosis.

2.2.6. *Effects of compound **2y** on reactive oxygen species in EC109 cells*

Through the above experiments, it was found that **2y** could cause activation of the mitochondrial apoptotic pathway and cause a caspase cascade reaction, leading to apoptosis. ROS are closely related to endogenous apoptosis, and a rise in ROS can lead to mitochondrial damage and mediate apoptosis [30,36,37]. In this study, we examined the effects of **2y** on intracellular ROS levels (at 24 h), and the ROS level significantly increased after treatment with 1.5 μM and 3 μM **2y** (Fig. 6). This experimental result further confirms previous studies showing that oxidative stress leads to apoptosis in EC109 cells.

2.2.7. *Effects of compound **2y** on ROS-Related pathway proteins in EC109 cells*

A rise in ROS can lead to changes in stress proteins [38–40]. In

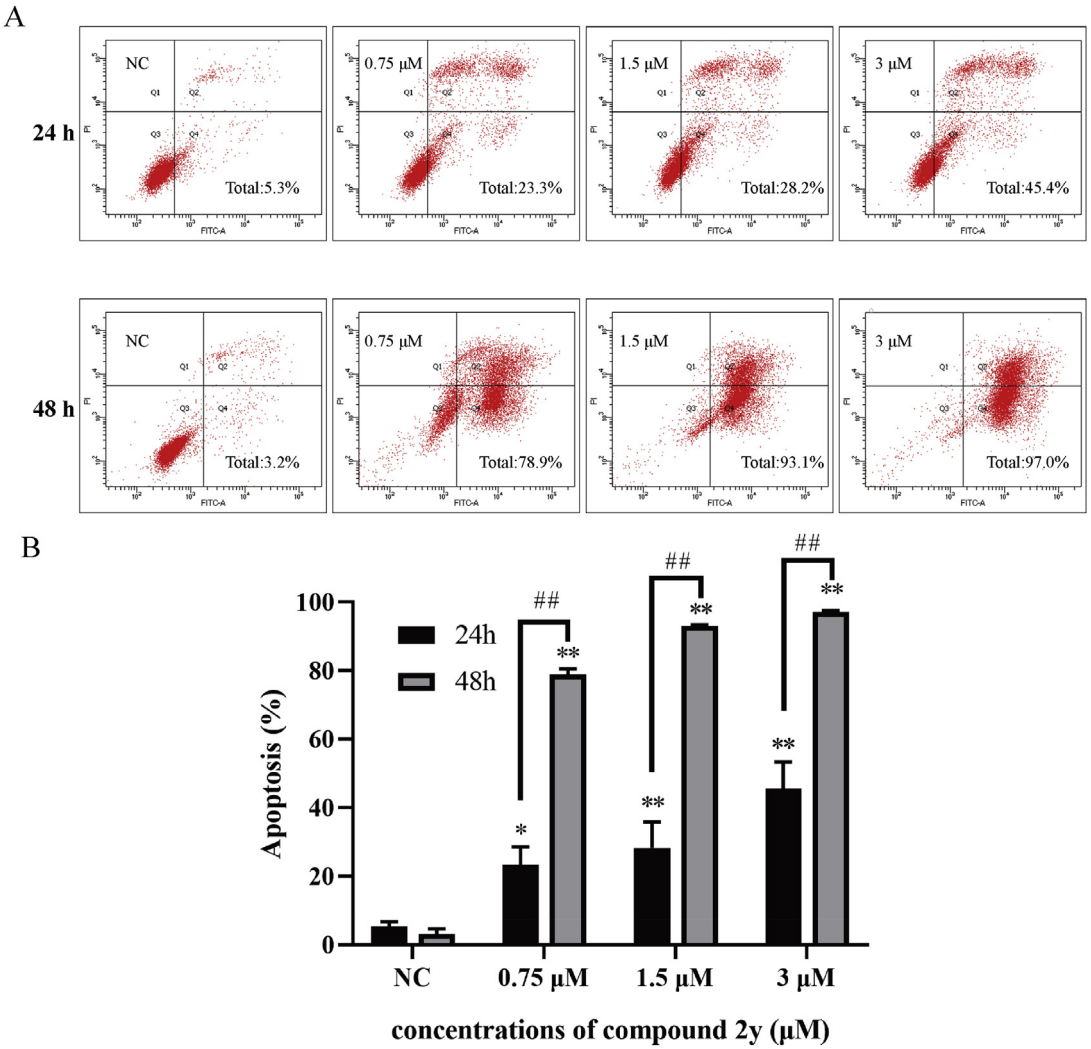

Fig. 3. Compound **2y** induced apoptosis of EC109 cells (A) Incubate with different concentrations of compound **2y** (0, 0.75, 1.5 and 3 μM). After incubated with **2y** for 24h and 48h, EC109 cells were detected by Annexin V/PI with flow cytometric analysis. The Q3 represents live cells, Q4 represents early/primary apoptotic cells, Q2 represents late/secondary apoptotic cells and Q1 represents cells necrosis. (B) The percentage of apoptosis (early and late apoptosis) cells increased dependently with various concentrations of **2y**. Date are represented as mean ± SD of three independent experiments. *$p < 0.05$ verse control, **$p < 0.01$ verse control.

addition, the upregulation of p-ASK1 could activate MKK4 and JNK [38,41], and JNK can be activated to regulate p-c-jun (ser63) [42]. In this research, Western Blotting was used to detect changes in related pathway proteins. As shown in Fig. 7, we found that p-ASK1 increased with the increase of drug concentration. In our study, p-MKK4 and p-JNK increase with increasing drug concentration. What is more, our experiment also proves that p-c-jun (ser63) is controlled and activated. Besides, p-JNK and p-c-jun (ser63) can regulate Bim to achieve the role of apoptosis [43]. These above results showed that compound 2y mediates apoptosis via the ROS pathway.

2.2.8. NAC affects the proliferative inhibitory effects of compound **2y** in EC109 cells

To explore the effects of excessive activation of ROS in EC109 cells, we introduced the antioxidant N-acetylcysteine (NAC). NAC can reduce superoxide anions, hydrogen peroxide and hydroxyl radicals to eliminate the influence of these types of free radicals on cells after entry into the cell [44–46]. After 4 h of pre-incubation with 5 mM NAC, the cells were incubated with **2y** for 24 h. As shown in Fig. 8, NAC completely reversed the effects of **2y** on the cells, and the survival rate was more than 90% at the highest dose of **2y**.

We continued to explore the effects of the compounds on cell clone formation ability. As shown in Fig. 8, NAC reversed the inhibitory effects of **2y** on the clonogenic capacity of EC109 cells at 0.5 μM. Cell morphology experiments found that the cells in the **2y**-treated group both contracted and rounded, and the number of cells decreased. In addition, the cells in the combination group and NC group remained the same. This experiment suggests that apoptosis induced by ROS may be the main pathway for this compound to inhibit cell proliferation.

2.2.9. Effects of NAC on **2y** on ROS, MMP and apoptosis

To further explore the effects of NAC on compound **2y**, flow cytometry was used to investigate the impact of **2y** on EC109 cells after 4 h of NAC intervention. As shown in Fig. 9, after the addition of NAC, the effects of **2y** on ROS, MMP and apoptosis in EC109 cells was reversed. Furthermore, compared with the NC group, there was no significant change. This result indicates that NAC clearance can indeed change the inhibition of **2y** in EC109 cells. Next, we need to explore the precise molecular mechanism of NAC reversing the

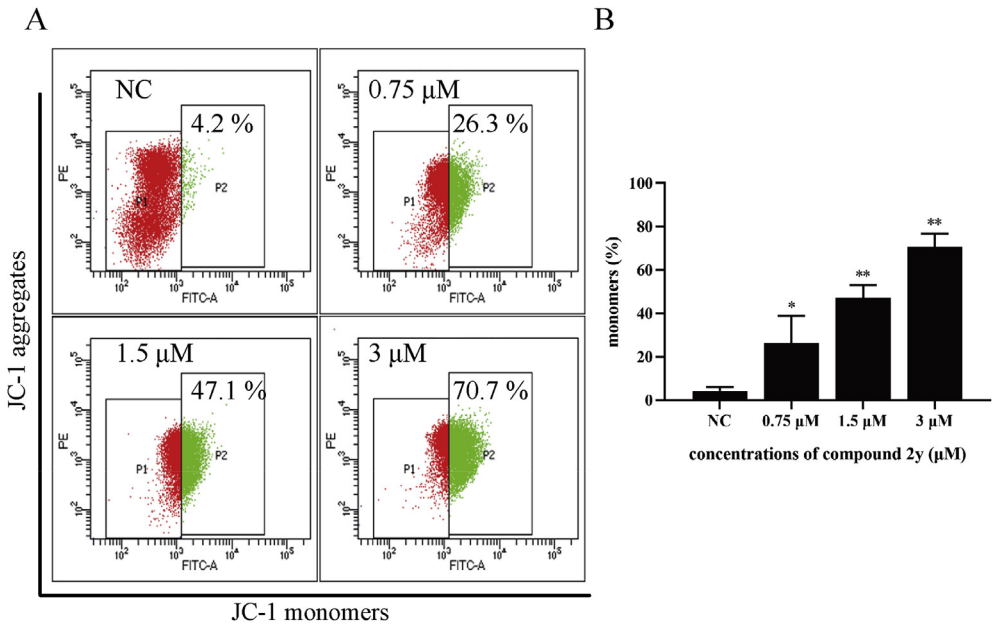

Fig. 4. (A) Changes of mitochondrial membrane potential at different drug concentrations (B) Statistical analysis of mitochondrial membrane potential changes. Date are represented as mean ± SD of three independent experiments. *$p < 0.05$ verse control, **$p < 0.01$ verse control.

effects of **2y**.

*2.2.10. NAC affects the protein expression changes of compound **2y** on ROS pathway and apoptotic pathway*

Western blotting was used to further explore the molecular mechanism of the effects of **2y** after NAC scavenging ROS in EC109 cells. As shown in Fig. 10, after the addition of NAC, the effects of **2y** on ROS-related proteins (p-ASK1, p-MKK4, and p-JNK) in EC109 cells was reversed. Compared with the NC group, there was no significant change. This result indicates that ROS clearance does indeed block **2y**-mediated expression of related ROS pathway proteins in EC109 cells.

We then further detected the expression of apoptosis-related proteins, as shown in Fig. 10. After co-treatment with NAC (5 mM) and **2y** (3 μM), expression of the anti-apoptotic protein Bcl-2 was significantly higher than that after treatment with **2y** (3 μM) alone. Moreover, there was no significant change compared with the NC group. Further experiments revealed that NAC inhibited the cleavage of caspase 9 and led to a decrease in cleaved caspase 3. In conclusion, NAC eradication of ROS can lead to a loss of **2y** regulation of apoptosis in EC109 cells. It was further proven that **2y** inhibits the proliferation of tumour cells by increasing intracellular ROS levels.

2.3. In vivo

*2.3.1. Compound **2y** inhibits the growth of transplanted tumours in nude mice*

The above experiments elucidated the specific molecular mechanism of **2y** in vitro. To further explore the antitumour effects of compound **2y** in vivo, we constructed a xenograft tumour model in nude mice by using EC109 cells. As shown in Fig. 11, there was no significant difference in tumour volumes between the three groups initially, and until the 5th day, the tumour growth rate in the drug treatment groups began to be lower than that in the NC group. At the same time, the growth rate of the high-dose group was slower than that of the low-dose group. There was a significant difference between the high-dose group and the NC group after eight days. On the 10th day, there was also a substantial difference between the low-dose and NC groups.

After 14 days of continuous treatment, the NC group's tumour volume reached nearly 1500 mm^3, while some nude mice showed local necrosis. Therefore, it was decided to end treatment, and the tumour tissue was removed and weighed. As shown in Fig. 11, the average tumour weights in the two drug groups were significantly smaller than that in the NC group. Moreover, the mean tumour weight in the high-dose group was the lowest of the three groups. This result indicates that both high and low doses of **2y** have inhibitory effects on tumours. Additionally, the body weights of the nude mice were not significantly different among the three groups, suggesting low toxicity of compound **2y**.

*2.3.2. Compound **2y** induces apoptosis of oesophageal cancer EC109 in vivo*

The tumour tissues were sectioned, and HE staining was used to detect the pathological morphology of the tumour tissues. The NC group showed a trend of cluster growth, with an intact morphology and no abnormalities, and the overall cell arrangement was relatively close (Fig. 12F). However, in the drug delivery groups, there was apparent cellular loosening and morphological changes. The number of cells was also reduced compared with that in the NC group, while the nucleus showed shrinkage. The above experiments preliminarily proved that **2y** inhibited tumour tissue in vivo.

To further explore the mechanism of **2y**, we homogenized the tumour tissue, the extracted protein and performed Western blotting experiments to verify the specific mechanism of **2y** in vivo. As shown in Fig. 12, compared with the NC group, the expression of Bcl-2 decreased significantly. There was no significant change between Bax expression in the low-dose group and NC group; there was only a significant difference between the high-dose group and NC group, but the ratio of Bax to Bcl-2 increased with increasing drug concentration. There was a significant difference in the Bax/Bcl-2 ratio in the low-dose group and the high-dose group. In addition, in the high-dose group, the expression levels of Cyto C, cleaved caspase 9, and cleaved caspase 3 were significantly different from those in the NC group. In summary, **2y** affects the

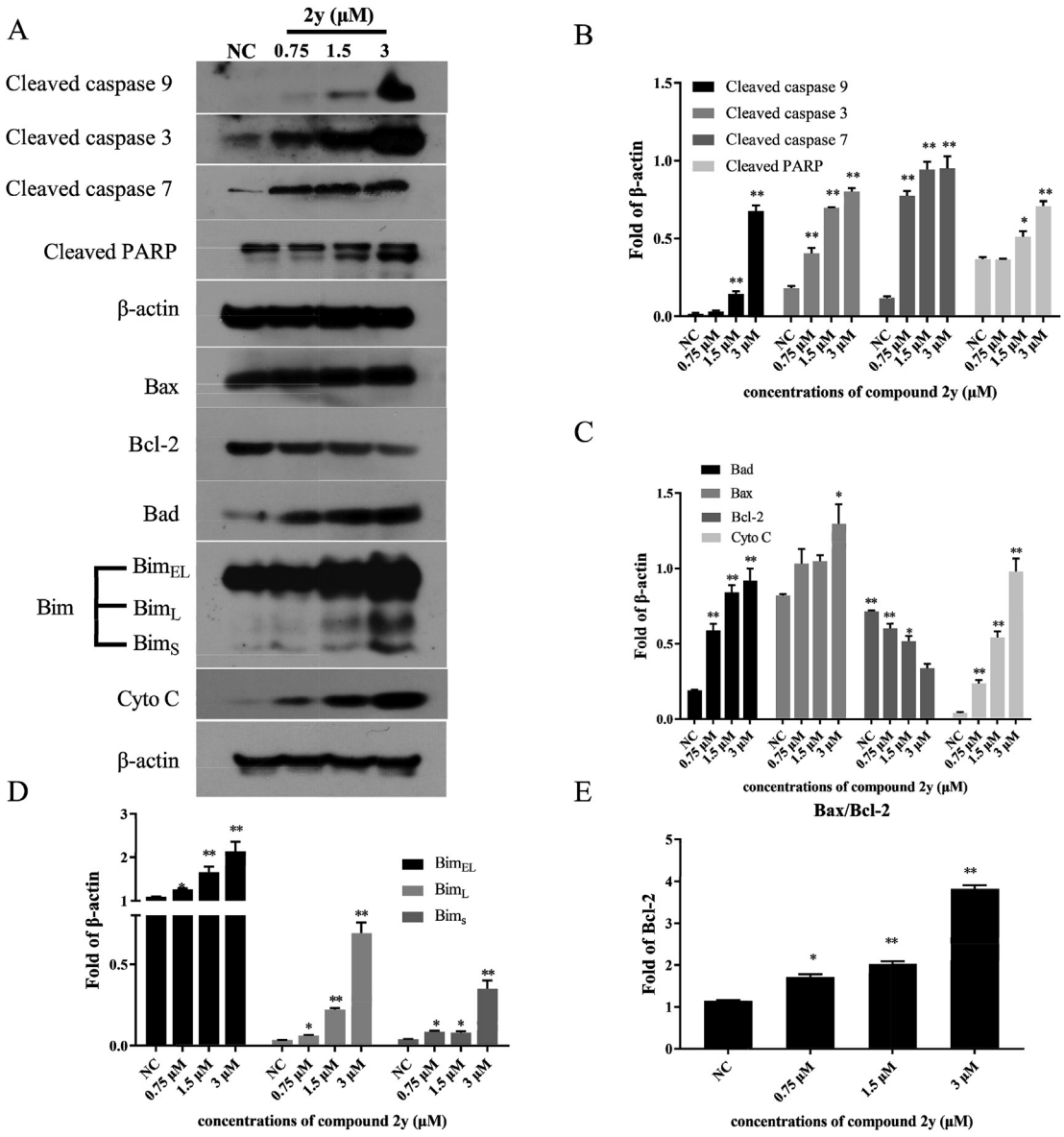

Fig. 5. (A) The expression of Bcl-2 family and Caspase family related proteins were detected by western blotting. (B) The density ratio of proteins after treatment with compound **2y**. (C) The expression of Bad, Bax, Bcl-2, Bim, Cyto C and β-Actin were detected by western blotting. (D) Expression of three isoform proteins of Bim. (E) Ratio of Bax to Bcl-2. The β-Actin was used as control. Date are represented as mean ± SD of three independent experiments. *$p < 0.05$ verse control, **$p < 0.01$ verse control.

mitochondrial pathway in vivo, eventually leading to apoptosis and thereby inhibiting the growth and development of tumour tissue, which is consistent with the molecular mechanism in vitro.

As shown in Fig. 12, we found significant changes in ROS-related proteins (p-ASK1, p-MKK4, and p-JNK). This result indicates that **2y** promotes apoptosis through the ROS pathway in vivo.

2.3.3. Study on the in vivo toxicity of compound *2y*

Previous studies demonstrated that compound **2y** has an inhibitory effect on tumour tissues in vivo. Nevertheless, an ideal clinical medication should have absolute safety. From the state of experimental animals, it can be seen from Fig. 13 that after 14 days of treatment, there was no significant difference in body weight among the groups.

To further explore the changes in specific safety indicators, biochemical blood indicators were used to detect potential pathological changes. As shown in Table 2, there was no significant difference between the drug group and NC group, and all parameters were close to those in the NC group, which indicated that compound **2y** did not cause changes in biochemical blood indicators in each group. This result further demonstrates that compound **2y** has low toxicity.

In order to further explore liver and kidney function, we found no significant difference in creatinine content and uric acid content between the treated group and the NC group (Fig. 13).

After treatment, we dissected the nude mice, and there were no visible abnormalities in the related organs. Finally, we performed HE staining on the organs and tissues of the nude mice. As shown in Fig. 13, the distribution of red pulp and white pulp in the spleen did not significantly increase or decrease compared with that in the NC group. The precise boundary of glomeruli in the kidneys was not substantially different from that in the NC group, and there were no abnormalities in the heart, lungs, or liver. This result indicated that **2y** was less toxic to nude mice.

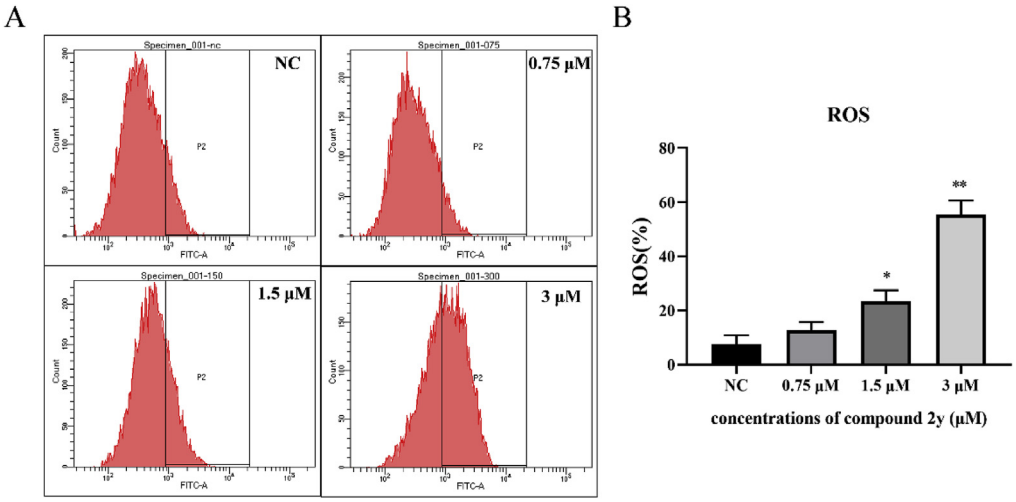

Fig. 6. (A) The production of ROS was tested by the ROS-detecting fluorescent dye DCF-DA in combination with flow cytometry. (B) The rate of ROS generation after treatment with different concentrations of compound **2y** by 24h. (0, 0.75, 1,5 and 3 μM). *$p < 0.05$ verse control, **$p < 0.01$ verse control.

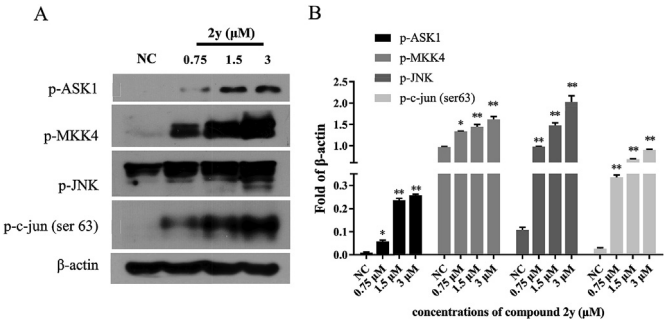

Fig. 7. (A) The expression of p-ASK1, p-MKK4, p-JNK, p-CJUN (ser63) and β-Actin were detected by western blotting. (B) The density ratio of proteins after treatment with compound **2y**. The β-Actin was used as control. Date are represented as mean ± SD of three independent experiments. *$p < 0.05$ verse control, **$p < 0.01$ verse control.

3. Conclusion

Overall, a series of novel derivatives of flexicaulin A (FA) condensed with aromatic rings were designed, synthesized and evaluated for their anticancer activities against four selected human cancer cell lines. Most of the synthesized compounds showed enhanced antiproliferative activities compared with FA and oridonin against all four selected cancer lines. Among all of the compounds, compound **2y** with a 4-(chloromethyl) benzoic acid moiety was found to possess the best antiproliferative activity. It was suspected that the introduction of aromatic rings could increase the anticancer activity of these compounds.

Further mechanistic studies indicated that compound **2y** mainly relied on an excessive accumulation of ROS to induce apoptosis. Compound **2y** regulates downstream apoptosis by upregulating p-ASK1, p-JNK, p-MKK4, and p-c-jun (ser63) in the ROS/JNK pathway. Moreover, **2y** further upregulated Bim and Bad and downregulated Bcl-2, which ultimately led to the release of cytochrome C. Finally, caspase 9, caspase 7, caspase 3, and PARP were activated to induce cell apoptosis. In addition, NAC can reverse apoptosis caused by **2y**. Xenograft tumour experiments in nude mice proved that **2y** has a visible antitumour effect in vivo. The mechanism of **2y** is the promotion of the expression of the ROS-related proteins p-ASK1, p-JNK, and p-MKK4 in vivo. This results in an increase in the ratio of Bax to Bcl-2 and promotes the release of cytochrome C. Finally, **2y** activates caspase 9 and caspase 3. Further toxicity studies showed that there was no obvious damage to the organs of nude mice, and the biochemical blood indicators were not abnormal, which indicated that **2y** had low toxicity. In summary, these results indicate that compound **2y** holds promising potential as an antiproliferative agent with low toxicity.

4. Experimental

4.1. General

All commercially available starting materials and solvents were reagent grade and used without further purification. Reactions were monitored by thin-layer chromatography (TLC) on 0.25 mm silicagel plates (GF254) and visualized under UV light. Melting points were measured on an X-5 micro-melting apparatus and are uncorrected. ^{1}H NMR and ^{13}C NMR spectra were recorded on a Bruker 400 MHz and 100 MHz spectrometer, respectively. Waters Micro-mass Q-T of Micro-mass spectrometer by electrospray ionization (ESI) was used to acquire high-resolution mass spectra (HRMS) of all derivatives.

4.2. General procedure for the synthesis of ***compound 2a-2z***

FA (150 mg, 0.38 mmol) was dissolved in DCM (6 mL), then Bromobutyric acid, Phenylpropionic acid or different benzoic acids (0.76 mmol), EDCI (146 mg, 0.76 mmol) and DMAP (92 mg, 0.76 mmol) were added to stir for 4–6h at the room temperature. After completion of the reaction as indicated by TLC, the reaction mixture was poured into DCM (30 mL), and washed with water, brine, dried over anhydrous Na_2SO_4 and concentrated under vacuum, and then purified by column chromatography (PE/EA = 1:1, v/v) to afford **2a-2z** in 35%–65%.

4.2.1. (4aR,6R,6aR,9S,11S,11bS,12R,14R)-11b-(acetoxymethyl)-6,11-dihydroxy-4,4-dimethyl-8-methylene-7-oxotetradecahydro-6a,9-methanocyclohepta[a]naphthalen-12-yl-4-bromobutanoate (compound 2a)

White solid, yield: 56%; Mp: 136–137 °C. ^{1}H NMR (400 MHz, DMSO-d_6) δ 5.73 (s, 1H), 5.55 (s, 1H), 5.31 (s, 1H), 4.84 (d, J = 12.4 Hz, 1H), 4.37 (d, J = 12.3 Hz, 1H), 4.27 (t, J = 7.0 Hz, 2H), 3.50 (t, J = 6.8 Hz, 2H), 2.96 (d, J = 3.8 Hz, 1H), 2.54 (t, J = 4.2 Hz, 1H), 2.43 (t,

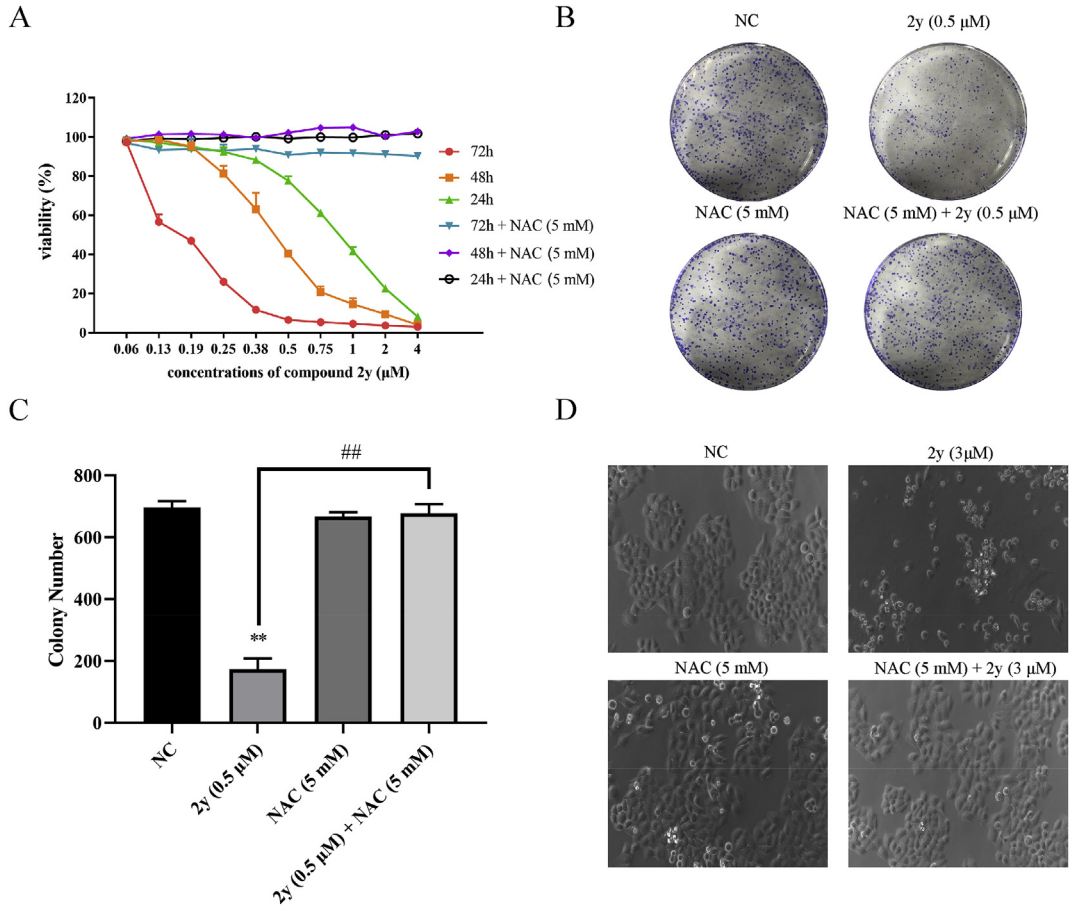

Fig. 8. (A) Changes in cell viability after introduction of NAC. (B) Changes in the formation of cell clones after the introduction of NAC. (C) The number of cell clones formed. (D) Cell morphology (200 ×). Date are represented as mean ± SD of three independent experiments. *$p < 0.05$ verse control, **$p < 0.01$ verse control.

J = 8.1 Hz, 2H), 2.27–2.21 (m, 2H), 2.17–2.12 (m, 1H), 2.08 (s, 3H), 2.01–1.92 (m, 3H), 1.86 (dd, J = 13.9, 4.0 Hz, 1H), 1.52 (s, 2H), 1.42 (t, J = 11.4 Hz, 3H), 1.05 (dd, J = 12.0, 3.0 Hz, 1H), 0.90 (s, 4H), 0.86 (s, 4H). ^{13}C NMR (100 MHz, DMSO-d_6) δ 204.2, 172.1, 170.2, 148.1, 112.8, 76.3, 71.9, 68.2, 66.0, 62.7, 61.8, 58.9, 52.8, 42.6, 41.1, 40.6, 34.1, 33.7, 32.7, 32.4, 27.7, 27.4, 22.1, 21.7, 20.7, 17.6. HR-MS(ESI): Calculated for $C_{26}H_{37}BrNaO_7$ [M+Na]$^+$: 563.1620, found 563.1686.

4.2.2. (4aR,6R,6aR,9S,11S,11bS,12R,14R)-11b-(acetoxymethyl)-6,11-dihydroxy-4,4-dimethyl-8-methylene-7-oxotetradecahydro-6a,9-methanocyclohepta[a]naphthalen-12-yl-3-phenylpropanoate (compound 2b)

White solid, yield: 63%; Mp: 143–144 °C. ^{1}H NMR (400 MHz, DMSO-d_6) δ 7.25 (t, J = 7.5 Hz, 2H), 7.18 (d, J = 7.5 Hz, 3H), 5.73 (s, 1H), 5.56 (s, 1H), 5.30 (s, 1H), 4.85 (d, J = 12.5 Hz, 1H), 4.43 (d, J = 4.3 Hz, 1H), 4.36 (d, J = 12.4 Hz, 1H), 4.28–4.25 (m, 1H), 2.91 (s, 1H), 2.76 (t, J = 7.4 Hz, 2H), 2.48–2.31 (m, 3H), 2.06 (d, J = 1.8 Hz, 3H), 1.96–1.83 (m, 2H), 1.73–1.58 (m, 3H), 1.55–1.34 (m, 5H), 1.09–1.03 (m, 1H), 0.91 (s, 4H), 0.86 (s, 4H). ^{13}C NMR (100 MHz, DMSO-d_6) δ 204.3, 172.35, 170.2, 148.0, 140.7, 128.2 (× 2), 128.1 (× 2), 125.8, 112.9, 76.2, 71.9, 66.0, 62.75, 61.8, 58.9, 52.9, 42.6, 41.1, 40.6, 38.9, 35.4, 33.7, 32.8, 32.4, 29.7, 27.7, 22.1, 20.7, 17.7. HR-MS(ESI): Calculated for $C_{31}H_{41}O_7$ [M+H]$^+$: 525.2852, found 525.2740.

4.2.3. (4aR,6R,6aR,9S,11S,11bS,12R,14R)-11b-(acetoxymethyl)-6,11-dihydroxy-4,4-dimethyl-8-methylene-7-oxotetradecahydro-6a,9-methanocyclohepta[a]naphthalen-12-yl-benzoate. (compound 2c)

White solid, yield: 60%; Mp: 124–125 °C. ^{1}H NMR (400 MHz, DMSO-d_6) δ 7.84 (d, J = 7.9 Hz, 2H), 7.61 (t, J = 7.3 Hz, 1H), 7.49 (t, J = 7.7 Hz, 2H), 5.86 (s, 2H), 5.42 (s, 1H), 4.94 (d, J = 12.3 Hz, 1H), 4.53 (d, J = 12.5 Hz, 1H), 4.37 (d, J = 4.3 Hz, 2H), 3.14 (d, J = 3.6 Hz, 1H), 2.65 (dt, J = 13.8, 4.1 Hz, 1H), 2.15 (s, 3H), 2.03–1.93 (m, 2H), 1.86–1.60 (m, 4H), 1.49 (q, J = 16.5, 14.5 Hz, 4H), 1.14 (d, J = 11.7 Hz, 1H), 0.99 (d, J = 12.4 Hz, 1H), 0.94 (s, 3H), 0.93 (s, 4H). ^{13}C NMR (100 MHz, DMSO-d_6) δ 204.1, 170.2, 165.9, 148.3, 132.5, 130.9, 129.2 (× 2), 128.1 (× 2), 112.8, 76.9, 72.0, 66.0, 62.80, 62.0, 59.1, 52.9, 42.9, 41.1, 40.6, 38.9, 33.7, 32.9, 32.5, 27.9, 22.2, 20.7, 17.7. HR-MS(ESI): Calculated for $C_{29}H_{36}NaO_7$ [M+Na]+: 519.2359, found 519.2390.

4.2.4. (4aR,6R,6aR,9S,11S,11bS,12R,14R)-11b-(acetoxymethyl)-6,11-dihydroxy-4,4-dimethyl-8-methylene-7-oxotetradecahydro-6a,9-methanocyclohepta[a]naphthalen-12-yl-2-fluorobenzoate. (compound 2d)

White solid, yield: 55%; Mp: 145–147 °C. ^{1}H NMR (400 MHz, DMSO-d_6) δ 7.70 (td, J = 7.7, 1.9 Hz, 1H), 7.58 (tdd, J = 7.0, 4.9, 1.9 Hz, 1H), 7.28–7.21 (m, 2H), 5.78 (s, 2H), 5.34 (s, 1H), 4.89 (d, J = 12.5 Hz, 1H), 4.49–4.42 (m, 2H), 4.32 (d, J = 1.9 Hz, 1H), 3.11–3.06 (m, 1H), 2.60 (dt, J = 14.1, 4.2 Hz, 1H), 2.11 (s, 3H), 2.01–1.88 (m, 2H), 1.76 (q, J = 12.5 Hz, 1H), 1.62 (d, J = 25.1 Hz, 2H), 1.53–1.38 (m, 3H), 1.34–1.14 (m, 2H), 1.12–1.06 (m, 1H), 0.99–0.92 (m, 1H), 0.90 (s, 3H), 0.88 (s, 4H). ^{13}C NMR (100 MHz, DMSO-d_6) δ 204.0, 170.3, 163.1, 159.5, 148.1, 134.3, 132.05, 124.0, 119.3, 116.4, 112.8, 77.2, 72.0, 66.1,

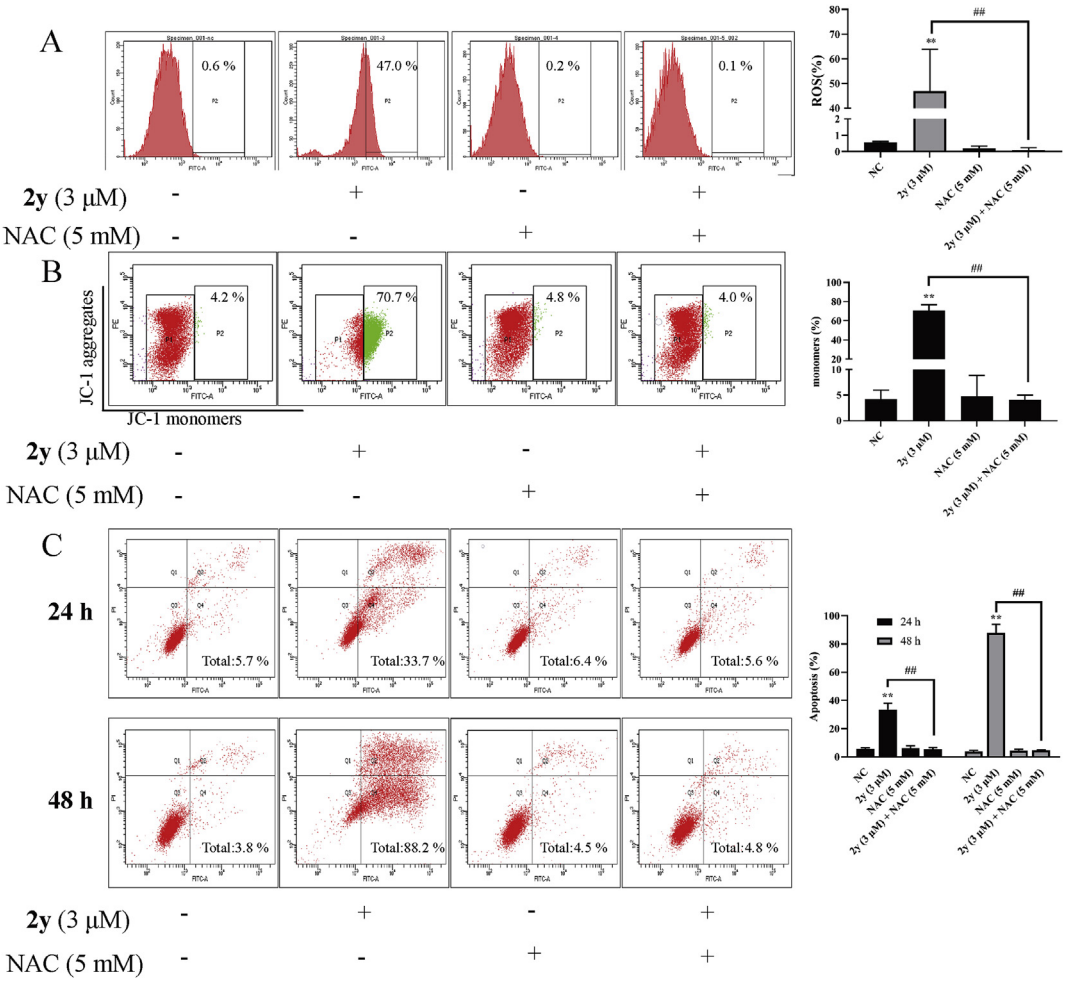

Fig. 9. (A) Changes of intracellular reactive oxygen species after the introduction of NAC. (B) Changes of mitochondrial membrane potential in cells after the introduction of NAC. (C) Changes in apoptosis after the introduction of NAC. Date are represented as mean ± SD of three independent experiments. *$p < 0.05$ verse control, **$p < 0.01$ verse control.

62.7, 61.9, 59.1, 52.8, 42.8, 41.1, 40.6, 38.9, 33.7, 32.8, 32.5, 27.9, 22.2, 20.7, 17.7. HR-MS(ESI): Calculated for $C_{29}H_{35}FNaO_7$ $[M+Na]^+$: 537.2265, found 537.2253.

4.2.5. (4aR,6R,6aR,9S,11S,11bS,12R,14R)-11b-(acetoxymethyl)-6,11-dihydroxy-4,4-dimethyl-8-methylene-7-oxotetradecahydro-6a,9-methanocyclohepta[a]naphthalen-12-yl-2-chlorobenzoate. (compound 2e)

White solid, yield: 42%; Mp: 146–147 °C. ^{1}H NMR (400 MHz, DMSO-d_6) δ 7.70 (d, J = 7.8 Hz, 1H), 7.51–7.47 (m, 2H), 7.36 (dt, J = 8.3, 4.3 Hz, 1H), 5.78 (d, J = 14.6 Hz, 2H), 5.32 (s, 1H), 4.92 (d, J = 12.4 Hz, 1H), 4.57 (dd, J = 4.3, 1.7 Hz, 1H), 4.45 (d, J = 12.5 Hz, 1H), 4.30 (d, J = 2.0 Hz, 1H), 3.08 (d, J = 3.9 Hz, 1H), 2.61 (dt, J = 14.1, 4.3 Hz, 1H), 2.11 (d, J = 1.8 Hz, 3H), 1.98–1.86 (m, 2H), 1.77 (q, J = 12.4 Hz, 1H), 1.68–1.58 (m, 2H), 1.54–1.29 (m, 4H), 1.24 (dd, J = 11.1, 5.2 Hz, 1H), 1.10 (d, J = 10.7 Hz, 1H), 0.94 (d, J = 8.8 Hz, 1H), 0.91 (s, 3H), 0.88 (s, 4H). ^{13}C NMR (100 MHz, DMSO-d_6) δ 203.9, 170.3, 164.4, 148.0, 132.6, 132.0, 130.4, 130.3, 126.7, 112.9, 77.6, 72.1, 66.1, 62.7, 61.9, 59.2, 52.8, 42.8, 41.2, 40.6, 38.9, 33.7, 32.9, 32.9, 32.5, 27.8, 22.2, 20.8, 17.7. HR-MS(ESI): Calculated for $C_{29}H_{35}ClNaO_7$ $[M+Na]^+$: 553.1969, found 553.2032.

4.2.6. (4aR,6R,6aR,9S,11S,11bS,12R,14R)-11b-(acetoxymethyl)-6,11-dihydroxy-4,4-dimethyl-8-methylene-7-oxotetradecahydro-6a,9-methanocyclohepta[a]naphthalen-12-yl-2-bromobenzoate. (compound 2f)

White solid, yield: 57%; Mp: 143–144 °C. ^{1}H NMR (400 MHz, DMSO-d_6) δ 7.69–7.65 (m, 2H), 7.43–7.37 (m, 2H), 5.81–5.78 (m, 1H), 5.75 (d, J = 5.3 Hz, 2H), 5.32 (s, 1H), 4.93 (d, J = 12.5 Hz, 1H), 4.61 (d, J = 4.3 Hz, 1H), 4.43 (d, J = 12.4 Hz, 1H), 4.32 (d, J = 2.0 Hz, 1H), 3.13–3.08 (m, 1H), 2.61 (dt, J = 13.8, 4.0 Hz, 1H), 2.12 (s, 3H), 1.97–1.87 (m, 2H), 1.83–1.57 (m, 4H), 1.44 (td, J = 18.6, 16.6, 10.8 Hz, 3H), 1.10 (dd, J = 12.8, 2.3 Hz, 1H), 0.94 (d, J = 8.9 Hz, 1H), 0.91 (s, 3H), 0.88 (s, 4H). ^{13}C NMR (100 MHz, DMSO-d_6) δ 203.9, 170.3, 165.0, 148.0, 133.5, 132.6, 132.4, 132.0, 127.2, 120.5, 113.0, 77.7, 72.1, 66.1, 62.7, 61.9, 59.2, 54.8, 52.8, 42.7, 41.2, 40.6, 33.7, 32.9, 32.5, 27.8, 22.2, 20.8, 17.7. HR-MS(ESI): Calculated for $C_{29}H_{35}BrNaO_7$ $[M+Na]^+$: 597.1464, found 597.1508.

4.2.7. (6R,6aR,9S,11S,11bS,12R)-11b-(acetoxymethyl)-6,11-dihydroxy-4,4-dimethyl-8-methylene-7-oxotetradecahydro-6a,9-methanocyclohepta[a]naphthalen-12-yl-2-methylbenzoate. (compound 2g)

White solid, yield: 46%; Mp: 134–135 °C. ^{1}H NMR (400 MHz, DMSO-d_6) δ 7.72–7.67 (m, 1H), 7.37 (td, J = 7.5, 1.6 Hz, 1H), 7.21 (d, J = 7.7 Hz, 2H), 5.78 (d, J = 10.2 Hz, 2H), 5.33 (s, 1H), 4.91 (d, J = 12.4 Hz, 1H), 4.48 (d, J = 12.2 Hz, 1H), 4.42 (d, J = 4.4 Hz, 1H), 4.29

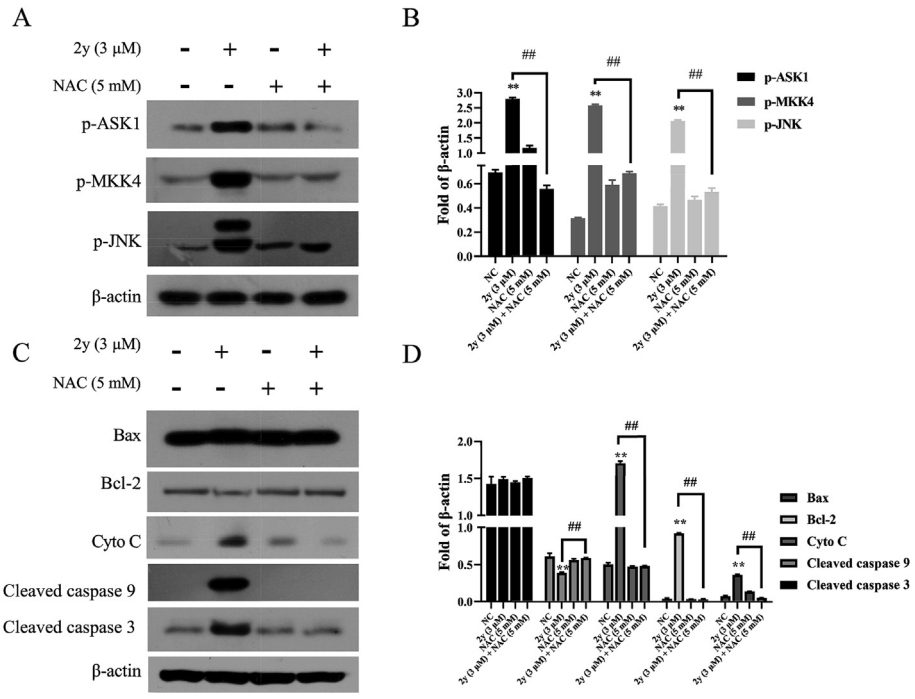

Fig. 10. (A) Changes of intracellular ROS-related protein after the introduction of NAC. (B) ROS-related protein expression. (C) Changes of apoptosis-related proteins in cells after the introduction of NAC. (D) Apoptosis-related protein expression. The β-Actin was used as control. Date are represented as mean ± SD of three independent experiments. *$p < 0.05$ verse control, **$p < 0.01$ verse control.

(d, J = 2.0 Hz, 1H), 3.08 (d, J = 3.9 Hz, 1H), 2.60 (dt, J = 14.2, 4.2 Hz, 1H), 2.44 (s, 3H), 2.11 (s, 3H), 1.98−1.87 (m, 2H), 1.80 (q, J = 12.7 Hz, 1H), 1.66−1.56 (m, 2H), 1.54−1.32 (m, 4H), 1.31−1.21 (m, 1H), 1.09 (d, J = 10.8 Hz, 1H), 0.97−0.92 (m, 1H), 0.90 (s, 3H), 0.89 (s, 4H). ^{13}C NMR (100 MHz, DMSO-d_6) δ 204.1, 170.3, 166.9, 148.5, 138.9, 131.4, 131.1, 130.6, 130.4, 125.3, 112.6, 76.9, 72.0, 66.1, 62.8, 62.0, 59.2, 52.9, 43.0, 41.2, 40.6, 38.9, 33.7, 32.9, 32.5, 27.9, 22.2, 21.0, 20.7, 17.7. HR-MS(ESI): Calculated for $C_{30}H_{38}NaO_7$ $[M+Na]^+$: 533.2595, found 533.2595.

4.2.8. (4aR,6R,6aR,9S,11S,11bS,12R,14R)-11b-(acetoxymethyl)-6,11-dihydroxy-4,4-dimethyl-8-methylene-7-oxotetradecahydro-6a,9-methanocyclohepta[a]naphthalen-12-yl-2-(trifluoromethyl) benzoate. (compound 2h)

White solid, yield: 52%; Mp: 136−137 °C. ^{1}H NMR (400 MHz, DMSO-d_6) δ 7.78 (t, J = 8.8 Hz, 2H), 7.70 (dd, J = 6.3, 2.7 Hz, 2H), 5.81 (s, 1H), 5.73 (s, 1H), 5.30 (s, 1H), 4.93 (d, J = 12.5 Hz, 1H), 4.68 (d, J = 4.0 Hz, 1H), 4.39 (d, J = 12.5 Hz, 1H), 4.34 (s, 1H), 3.05 (s, 1H), 2.63−2.54 (m, 1H), 2.11 (s, 3H), 1.93 (d, J = 14.4 Hz, 2H), 1.81−1.65 (m, 2H), 1.59 (s, 2H), 1.43 (t, J = 16.9 Hz, 3H), 1.17 (d, J = 11.4 Hz, 1H), 1.11 (d, J = 12.4 Hz, 1H), 0.95 (s, 1H), 0.91 (s, 3H), 0.89 (s, 4H). ^{13}C NMR (100 MHz, DMSO-d_6) δ 203.7, 170.3, 165.5, 147.8, 132.2, 131.3, 131.3, 130.8, 126.8, 126.1, 124.7, 122.04, 113.0, 78.1, 72.1, 66.0, 62.7, 61.9, 59.1, 52.8, 42.7, 41.2, 40.6, 33.7, 32.9, 32.5, 27.8, 22.2, 20.7, 17.7. HR-MS(ESI): Calculated for $C_{30}H_{35}F_3NaO_7$ $[M+Na]^+$: 587.2233, found 587.2208.

4.2.9. (4aR,6R,6aR,9S,11S,11bS,12R,14R)-11b-(acetoxymethyl)-6,11-dihydroxy-4,4-dimethyl-8-methylene-7-oxotetradecahydro-6a,9-methanocyclohepta[a]naphthalen-12-yl-2,3-dichlorobenzoate. (compound 2i)

White solid, yield: 58%; Mp: 145−146 °C. ^{1}H NMR (400 MHz, DMSO-d_6) δ 7.77 (dd, J = 8.0, 1.8 Hz, 1H), 7.63 (dd, J = 7.8, 1.7 Hz, 1H), 7.40 (t, J = 8.0 Hz, 1H), 5.78 (d, J = 18.8 Hz, 2H), 5.33 (s, 1H), 4.92 (d, J = 12.3 Hz, 1H), 4.66 (d, J = 4.1 Hz, 1H), 4.43 (d, J = 12.5 Hz, 1H), 4.33 (d, J = 1.9 Hz, 1H), 3.10 (d, J = 4.1 Hz, 1H), 2.61 (dt, J = 14.1, 4.1 Hz, 1H), 2.12 (s, 3H), 1.97−1.88 (m, 2H), 1.83−1.58 (m, 4H), 1.54−1.36 (m, 4H), 1.10 (d, J = 10.7 Hz, 1H), 0.95 (t, J = 9.4 Hz, 1H), 0.91 (s, 3H), 0.88 (s, 4H). ^{13}C NMR (100 MHz, DMSO-d_6) δ 203.7, 170.3, 164.0, 147.9, 133.1, 133.0, 132.9, 132.6, 130.2, 129.8, 127.9, 113.1, 78.1, 72.1, 66.1, 62.7, 61.8, 59.1, 52.8, 42.7, 41.1, 40.6, 33.7, 32.8, 32.5, 27.8, 22.2, 20.8, 17.7. HR-MS(ESI): Calculated for $C_{29}H_{34}Cl_2NaO_7$ $[M+Na]^+$: 587.1579, found 587.1633.

4.2.10. (4aR,6R,6aR,9S,11S,11bS,12R,14R)-11b-(acetoxymethyl)-6,11-dihydroxy-4,4-dimethyl-8-methylene-7-oxotetradecahydro-6a,9-methanocyclohepta[a]naphth-alen-12-yl-2,4-dichlorobenzoate. (compound 2j)

White solid, yield: 61%; Mp: 133−134 °C. ^{1}H NMR (400 MHz, DMSO-d_6) δ 7.69 (d, J = 8.5 Hz, 2H), 7.50 (dd, J = 8.5, 2.0 Hz, 1H), 5.78 (d, J = 6.5 Hz, 2H), 5.33 (s, 1H), 4.91 (d, J = 12.4 Hz, 1H), 4.63 (d, J = 4.1 Hz, 1H), 4.43 (d, J = 12.3 Hz, 1H), 4.34−4.32 (m, 1H), 3.13−3.06 (m, 1H), 2.61 (dt, J = 14.3, 4.3 Hz, 1H), 2.11 (s, 3H), 2.03−1.85 (m, 2H), 1.80−1.55 (m, 3H), 1.52−1.27 (m, 4H), 1.24−1.07 (m, 2H), 0.95 (d, J = 6.0 Hz, 1H), 0.90 (s, 3H), 0.88 (s, 4H). ^{13}C NMR (100 MHz, DMSO-d_6) δ 203.8, 170.3, 163.6, 147.9, 136.7, 133.4, 132.3, 129.9, 129.0, 127.2, 113.1, 77.8, 72.0, 66.1, 62.7, 61.8, 59.1, 52.8, 42.7, 41.1, 40.6, 38.9, 33.7, 32.8, 32.5, 27.8, 22.2, 20.8, 17.7. HR-MS(ESI): Calculated for $C_{29}H_{34}Cl_2NaO_7$ $[M+Na]^+$: 587.1579, found 587.1564.

4.2.11. (4aR,6R,6aR,9S,11S,11bS,12R,14R)-11b-(acetoxymethyl)-6,11-dihydroxy-4,4-dimethyl-8-methylene-7-oxotetradecahydro-6a,9-methanocyclohepta[a]naph-thalen-12-yl 5-chloro-2-methoxybenzoate. (compound 2k)

White solid, yield: 57%; Mp: 133−135 °C. ^{1}H NMR (400 MHz, DMSO-d_6) δ 7.54−7.48 (m, 2H), 7.11 (d, J = 8.9 Hz, 1H), 5.77 (t, J = 1.2 Hz, 1H), 5.74 (d, J = 2.5 Hz, 2H), 5.32 (s, 1H), 4.89 (d, J = 12.4 Hz, 1H), 4.63 (d, J = 4.4 Hz, 1H), 4.43 (d, J = 12.3 Hz, 1H), 4.30 (d, J = 2.0 Hz, 1H), 3.78 (s, 3H), 3.04 (d, J = 4.3 Hz, 1H), 2.59 (dt, J = 13.8, 4.3 Hz, 1H), 2.10 (s, 3H), 1.97−1.86 (m, 2H), 1.78−1.69 (m, 1H), 1.66−1.57 (m, 2H), 1.53−1.33 (m, 4H), 1.12−1.06 (m, 1H), 0.94 (d, J = 9.7 Hz, 1H), 0.90 (s, 3H), 0.87 (s, 4H). ^{13}C NMR (100 MHz,

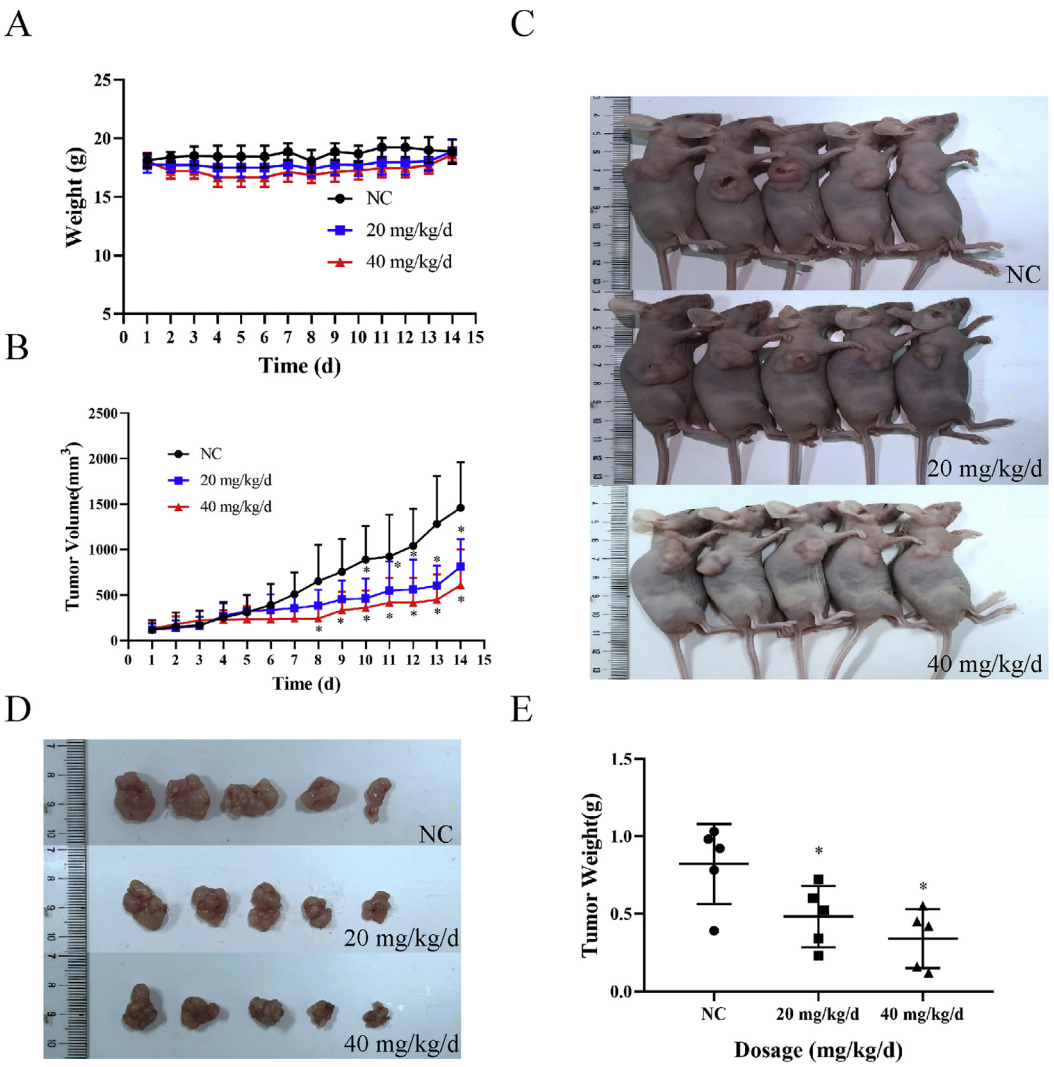

Fig. 11. (A) Nude mice weight during treatment. (B) Tumour volume in nude mice during treatment. (C) Photos of nude mice after 14 days of treatment. (D) Photographs of tumours in nude mice after 14 days of treatment. (E) Tumour weight in nude mice after 14 days of treatment. *$p < 0.05$ verse control, **$p < 0.01$ verse control.

DMSO-d_6) δ 204.0, 170.2, 163.4, 156.9, 148.1, 132.3, 130.5, 123.4, 122.2, 114.1, 112.9, 77.3, 72.1, 66.1, 62.7, 61.9, 59.1, 56.0, 54.8, 52.9, 42.8, 41.1, 40.6, 33.7, 32.9, 32.5, 27.8, 22.2, 20.7, 17.7. HR-MS(ESI): Calculated for $C_{30}H_{37}ClNaO_8$ $[M+Na]^+$: 583.2075, found 583.2157.

4.2.12. (4aR,6R,6aR,9S,11S,11bS,12R,14R)-11b-(acetoxymethyl)-6,11-dihydroxy-4,4-dimethyl-8-methylene-7-oxotetradecahydro-6a,9-methanocyclohepta[a]naph-thalen-12-yl-3-fluorobenzoate. (compound 2l)

White solid, yield: 58%; Mp: 124–125 °C. 1H NMR (400 MHz, DMSO-d_6) δ 7.64 (dt, J = 7.7, 1.4 Hz, 1H), 7.54–7.47 (m, 2H), 7.46–7.40 (m, 1H), 5.87–5.78 (m, 2H), 5.39 (s, 1H), 4.88 (d, J = 12.4 Hz, 1H), 4.48–4.42 (m, 2H), 4.34 (d, J = 2.0 Hz, 1H), 3.12–3.08 (m, 1H), 2.60 (dt, J = 13.9, 4.1 Hz, 1H), 2.11 (s, 3H), 1.99–1.87 (m, 2H), 1.74 (q, J = 12.7 Hz, 1H), 1.65–1.30 (m, 6H), 1.25–1.14 (m, 1H), 1.09 (dd, J = 12.7, 2.2 Hz, 1H), 0.98–0.92 (m, 1H), 0.90 (s, 3H), 0.88 (s, 4H). ^{13}C NMR (100 MHz, DMSO-d_6) δ 204.0, 170.2, 164.8, 162.8, 160.4, 148.2, 133.3, 130.5, 125.3, 119.6, 115.6, 112.9, 77.3, 72.0, 66.0, 62.7, 61.9, 59.1, 52.8, 42.8, 41.1, 40.6, 33.7, 32.9, 32.4, 27.8, 22.1, 20.7, 17.7. HR-MS(ESI): Calculated for $C_{29}H_{35}FNaO_7$ [M+Na]+: 537.2265, found 537.2253.

4.2.13. (4aR,6R,6aR,9S,11S,11bS,12R,14R)-11b-(acetoxymethyl)-6,11-dihydroxy-4,4-dimethyl-8-methylene-7-oxotetradecahydro-6a,9-methanocyclohepta[a]na-phthalen-12-yl-3-chlorobenzoate. (compound 2 m)

White solid, yield: 52%; Mp: 134–135 °C. ^{1}H NMR (400 MHz, DMSO-d_6) δ 7.76–7.72 (m, 2H), 7.67–7.63 (m, 1H), 7.50 (t, J = 7.9 Hz, 1H), 5.84–5.79 (m, 2H), 5.39 (s, 1H), 4.88 (d, J = 12.4 Hz, 1H), 4.48–4.42 (m, 2H), 4.34 (d, J = 1.6 Hz, 1H), 3.11 (d, J = 3.9 Hz, 1H), 2.59 (dt, J = 14.2, 4.3 Hz, 1H), 2.11 (s, 3H), 1.98–1.87 (m, 2H), 1.73 (q, J = 12.7 Hz, 1H), 1.61 (d, J = 13.7 Hz, 3H), 1.53–1.37 (m, 4H), 1.09 (dd, J = 12.6, 2.2 Hz, 1H), 0.97–0.92 (m, 1H), 0.89 (s, 3H), 0.87 (s, 4H). ^{13}C NMR (100 MHz, DMSO-d_6) δ 204.0, 170.2, 164.8, 148.1, 133.0, 132.9, 132.4, 130.3, 128.7, 127.8, 113.0, 77.4, 71.9, 66.0, 62.7, 61.9, 59.1, 52.8, 42.8, 41.1, 40.6, 38.9, 33.7, 32.9, 32.5, 27.8, 22.1, 20.7, 17.7. HR-MS(ESI): Calculated for $C_{29}H_{35}ClNaO_7$ $[M+Na]^+$: 553.1969, found 553.1976.

4.2.14. (4aR,6R,6aR,9S,11S,11bS,12R,14R)-11b-(acetoxymethyl)-6,11-dihydroxy-4,4-dimethyl-8-methylene-7-oxotetradecahydro-6a,9-methanocyclohepta[a]na-phthalen-12-yl-3-bromobenzoate. (compound 2n)

White solid, yield: 65%; Mp: 143–145 °C. ^{1}H NMR (400 MHz, DMSO-d_6) δ 7.92 (t, J = 1.9 Hz, 1H), 7.85–7.80 (m, 2H), 7.48 (t,

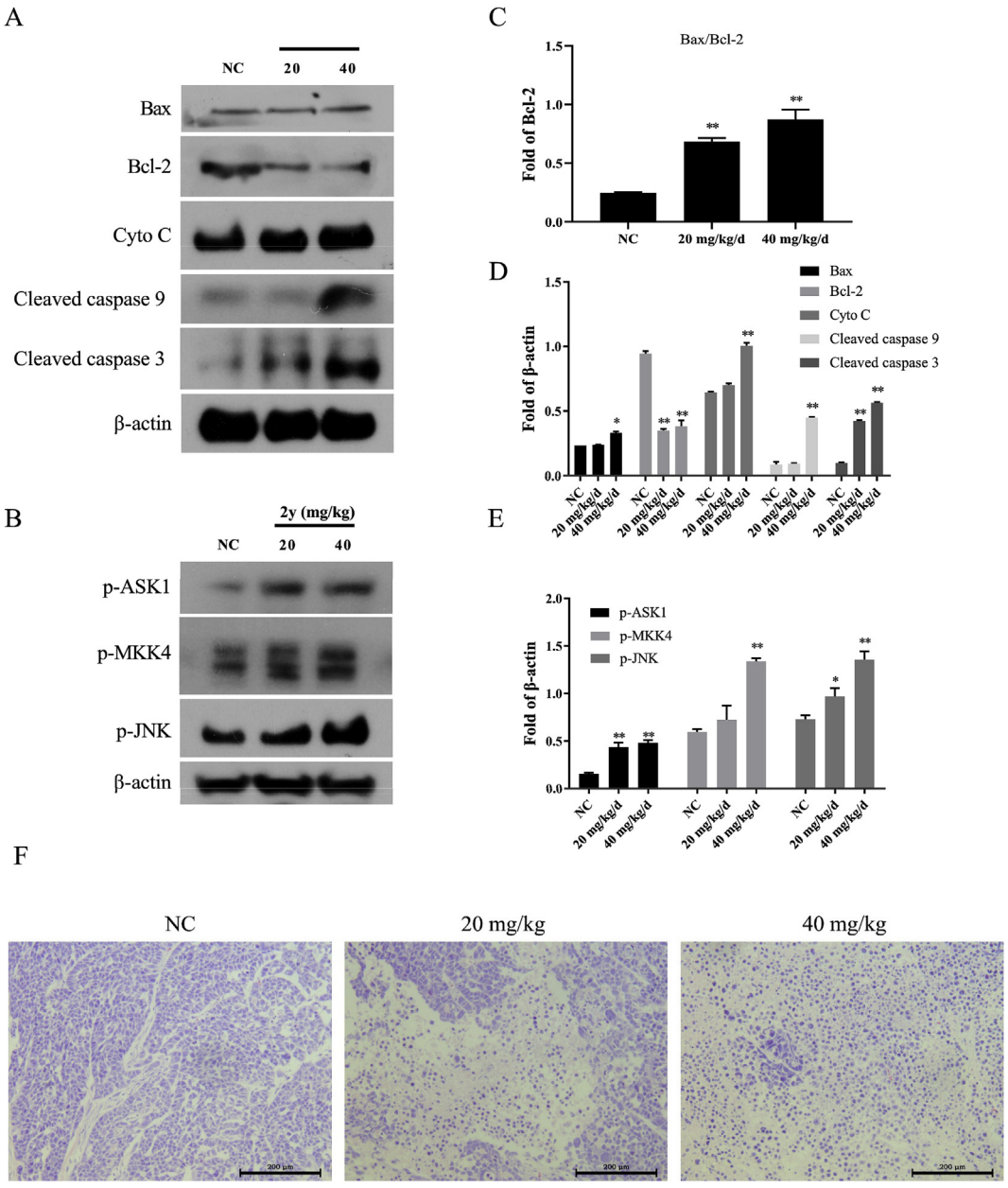

Fig. 12. (A) Apoptosis-related protein. (B) The ratio of Bax to Bcl-2. (C) Expression of apoptosis-related proteins. (D) ROS-related protein. (E) The expression level of ROS related protein. (F) Tumour sections in nude mice were stained with HE after 14 days of treatment. (200 ×) The β-Actin was used as control. Date are represented as mean ± SD of three independent experiments. *$p < 0.05$ verse control, **$p < 0.01$ verse control.

J = 7.9 Hz, 1H), 5.86 (d, J = 7.3 Hz, 2H), 5.44 (s, 1H), 4.93 (d, J = 12.4 Hz, 1H), 4.53–4.47 (m, 2H), 4.39–4.36 (m, 1H), 3.18–3.13 (m, 1H), 2.64 (dt, J = 14.1, 4.3 Hz, 1H), 2.15 (s, 3H), 2.03–1.93 (m, 2H), 1.83–1.62 (m, 4H), 1.59–1.41 (m, 4H), 1.13 (dd, J = 12.8, 2.0 Hz, 1H), 1.02–0.96 (m, 1H), 0.94 (s, 3H), 0.92 (s, 4H). ^{13}C NMR (100 MHz, DMSO-d_6) δ 204.0, 170.2, 164.7, 148.1, 135.2, 133.1, 131.6, 130.5, 128.2, 121.3, 112.9, 77.4, 71.9, 66.0, 62.7, 61.9, 59.1, 52.8, 42.8, 41.1, 40.6, 38.9, 33.7, 32.9, 32.5, 27.8, 22.1, 20.7, 17.7. HR-MS(ESI): Calculated for $C_{29}H_{35}BrNaO_7$ $[M+Na]^+$: 597.1464, found 597.1476.

4.2.15. (4aR,6R,6aR,9S,11S,11bS,12R,14R)-11b-(acetoxymethyl)-6,11-dihydroxy-4,4-dimethyl-8-methylene-7-oxotetradecahydro-6a,9-methanocyclohepta[a]na-phthalen-12-yl-3-methoxybenzoate. (compound 2°)

White solid, yield: 55%; Mp: 133–134 °C. ^{1}H NMR (400 MHz, DMSO-d_6) δ 7.36 (d, J = 6.8 Hz, 2H), 7.33–7.31 (m, 1H), 7.13 (dt, J = 6.7, 2.7 Hz, 1H), 5.80 (d, J = 8.7 Hz, 2H), 5.37 (s, 1H), 4.87 (d, J = 12.4 Hz, 1H), 4.47 (d, J = 12.5 Hz, 1H), 4.36 (d, J = 4.4 Hz, 1H), 4.33 (d, J = 2.4 Hz, 1H), 3.76 (s, 3H), 3.08 (d, J = 3.8 Hz, 1H), 2.59 (dt, J = 13.9, 4.3 Hz, 1H), 2.10 (s, 3H), 1.98–1.87 (m, 2H), 1.75 (q,

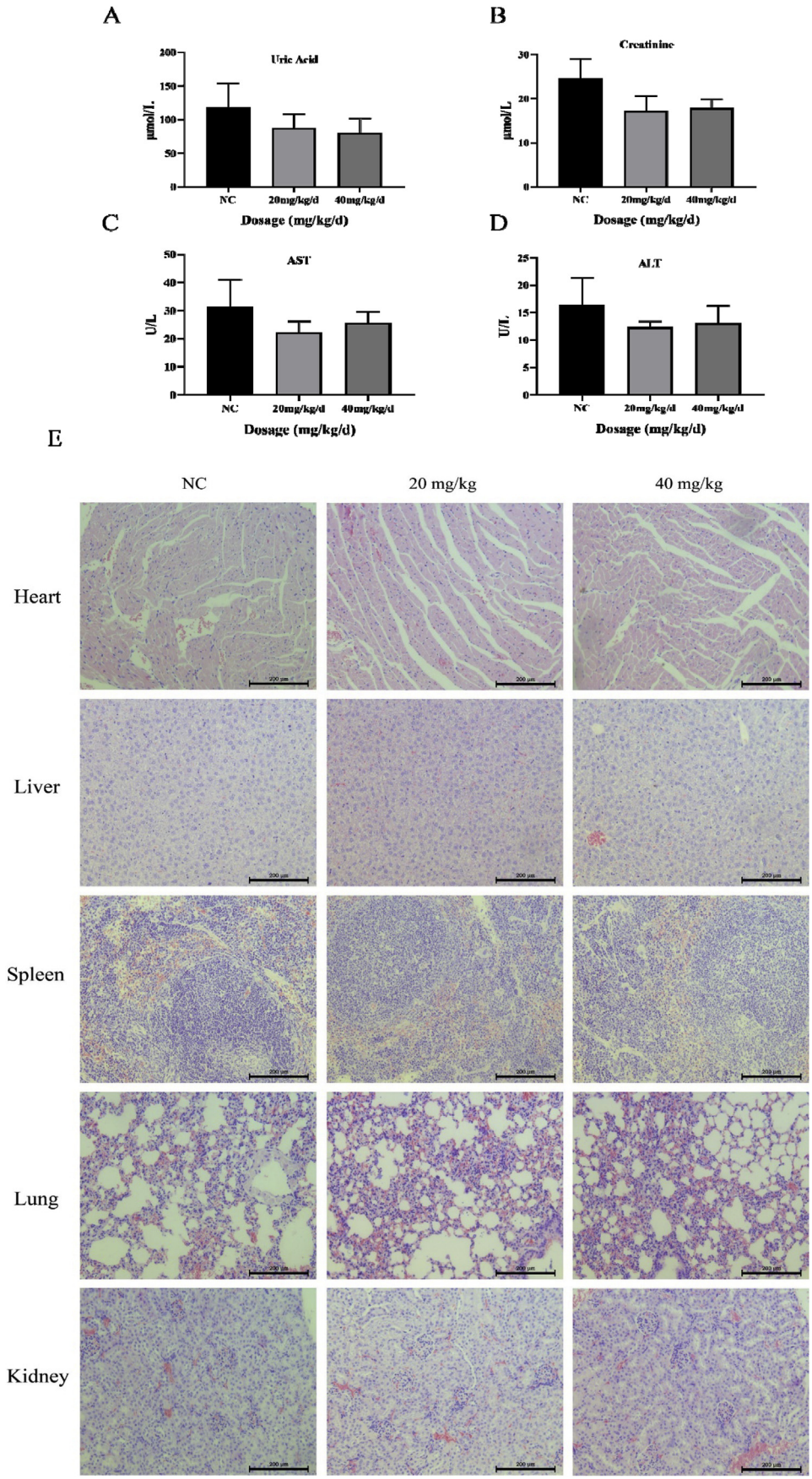

Fig. 13. (A) Changes in uric acid. (B) Changes in creatinine. (C) Changes in AST. (D) Changes in ALT. (E) After 14 days of treatment, the main organ sections of nude mice were stained with HE. (200 ×) Date are represented as mean ± SD of three independent experiments. *$p < 0.05$ verse control, **$p < 0.01$ verse control.

J = 12.7 Hz, 1H), 1.61 (d, J = 16.5 Hz, 3H), 1.54–1.35 (m, 4H), 1.09 (d, J = 12.9 Hz, 1H), 0.97–0.92 (m, 1H), 0.89 (s, 3H), 0.88 (s, 4H). ^{13}C NMR (100 MHz, DMSO-d_6) δ 204.1, 170.2, 165.7, 158.8, 148.3, 132.2, 129.3, 121.5, 118.0, 114.5, 112.7, 77.0, 72.0, 66.0, 62.7, 62.0, 59.1, 55.1, 52.9, 42.9, 41.1, 40.6, 38.9, 33.7, 32.9, 32.5, 27.9, 22.1, 20.7, 17.7. HR-MS(ESI): Calculated for $C_{30}H_{38}NaO_8$ $[M+Na]^+$: 549.2464, found 549.2485.

4.2.16. (4aR,6R,6aR,9S,11S,11bS,12R,14R)-11b-(acetoxymethyl)-6,11-dihydroxy-4,4-dimethyl-8-methylene-7-oxotetradecahydro-6a,9-methanocyclohepta[a]naph-thalen-12-yl-3-methylbenzoate. (compound 2p)

White solid, yield: 45%; Mp: 165–167 °C. ^{1}H NMR (400 MHz, DMSO-d_6) δ 7.63–7.56 (m, 2H), 7.37 (d, J = 7.8 Hz, 1H), 7.31 (t, J = 7.6 Hz, 1H), 5.80 (d, J = 4.9 Hz, 2H), 5.37 (s, 1H), 4.88 (d, J = 12.4 Hz, 1H), 4.48 (d, J = 12.4 Hz, 1H), 4.29 (dd, J = 7.3, 3.0 Hz, 2H), 3.08 (d, J = 3.6 Hz, 1H), 2.59 (dt, J = 14.2, 4.2 Hz, 1H), 2.31 (s, 3H), 2.10 (s, 3H), 1.97–1.87 (m, 2H), 1.76 (q, J = 12.5 Hz, 1H), 1.60 (d, J = 16.1 Hz, 2H), 1.54–1.33 (m, 4H), 1.31–1.20 (m, 1H), 1.08 (d, J = 11.0 Hz, 1H), 0.98–0.91 (m, 1H), 0.89 (s, 3H), 0.88 (s, 4H). ^{13}C NMR (100 MHz, DMSO-d_6) δ 204.1, 170.2, 166.0, 148.3, 137.3, 133.1, 130.9, 129.6, 128.0, 126.5, 112.8, 76.9, 72.0, 66.1, 62.8, 62.0, 59.1, 52.9, 42.9, 41.1, 40.6, 39.0, 33.7, 32.9, 32.5, 27.9, 22.1, 20.8, 20.7, 17.7. HR-MS(ESI): Calculated for $C_{30}H_{38}NaO_7$ $[M+Na]^+$: 533.2515, found 533.2556.

4.2.17. (4aR,6R,6aR,9S,11S,11bS,12R,14R)-11b-(acetoxymethyl)-6,11-dihydroxy-4,4-dimethyl-8-methylene-7-oxotetradecahydro-6a,9-methanocyclohepta[a]naph-thalen-12-yl-3-(trifluoromethyl) benzoate. (compound 2q)

White solid, yield: 57%; Mp: 143–144 °C. ^{1}H NMR (400 MHz, DMSO-d_6) δ 8.08–8.02 (m, 2H), 7.95 (d, J = 8.3 Hz, 1H), 7.72 (t, J = 7.8 Hz, 1H), 5.84 (d, J = 5.1 Hz, 2H), 5.40 (s, 1H), 4.89 (d, J = 12.5 Hz, 1H), 4.50–4.43 (m, 2H), 4.34 (s, 1H), 3.13 (s, 1H), 2.64–2.56 (m, 1H), 2.11 (s, 3H), 1.98–1.88 (m, 2H), 1.75 (q, J = 12.5 Hz, 1H), 1.62 (d, J = 12.7 Hz, 2H), 1.55–1.35 (m, 4H), 1.21–1.15 (m, 1H), 1.09 (d, J = 12.5 Hz, 1H), 0.95 (d, J = 14.2 Hz, 1H), 0.89 (s, 3H), 0.88 (s, 4H). ^{13}C NMR (100 MHz, DMSO-d_6) δ 204.0, 170.2, 164.8, 148.2, 133.1, 131.9, 129.7, 129.1, 125.4, 125.0, 122.3, 112.9, 77.5, 71.9, 66.0, 62.7, 61.9, 59.0, 52.8, 42.8, 41.1, 40.6, 38.9, 33.7, 32.9, 32.5, 27.8, 22.1, 20.7, 17.7. Calculated for $C_{30}H_{35}F_3NaO_7$ $[M+Na]^+$: 587.2233, found 587.2211.

4.2.18. (4aR,6R,6aR,9S,11S,11bS,12R,14R)-11b-(acetoxymethyl)-6,11-dihydroxy-4,4-dimeth-yl-8-methylene-7-oxotetradecahydro-6a,9-methanocyclohepta[a]naph-thalen-12-yl-3,4-dimethoxybenzoate. (compound 2r)

White solid, yield: 63%; Mp: 145–147 °C. ^{1}H NMR (400 MHz, DMSO-d_6) δ 7.41–7.36 (m, 2H), 6.99 (d, J = 8.4 Hz, 1H), 5.79 (d, J = 13.9 Hz, 2H), 5.36 (s, 1H), 4.86 (d, J = 12.3 Hz, 1H), 4.48 (d, J = 12.7 Hz, 1H), 4.30 (dd, J = 6.5, 3.1 Hz, 2H), 3.79 (s, 3H), 3.75 (s, 3H), 3.08 (d, J = 3.5 Hz, 1H), 2.59 (dt, J = 13.8, 4.0 Hz, 1H), 2.11 (s, 3H), 1.98–1.88 (m, 2H), 1.81–1.57 (m, 4H), 1.55–1.36 (m, 4H), 1.10 (d, J = 12.1 Hz, 1H), 0.94 (d, J = 12.5 Hz, 1H), 0.90 (s, 3H), 0.88 (s, 4H). ^{13}C NMR (100 MHz, DMSO-d_6) δ 204.2, 170.2, 165.6, 152.4, 148.4, 148.0, 123.2, 123.1, 112.6, 112.2, 110.8, 76.7, 72.1, 66.0, 62.8, 62.0, 59.7, 59.1, 55.6, 55.4, 52.9, 43.0, 41.1, 40.6, 33.7, 32.9, 32.5, 27.9, 22.1, 20.7, 17.7. HR-MS(ESI): Calculated for $C_{31}H_{40}NaO_9$ $[M+Na]^+$: 579.2570, found 579.2644.

4.2.19. (4aR,6R,6aR,9S,11S,11bS,12R,14R)-11b-(acetoxymethyl)-6,11-dihydroxy-4,4-dimethyl-8-methylene-7-oxotetradecahydro-6a,9-methanocyclohepta[a]naph-thalen-12-yl-4-fluorobenzoate. (compound 2s)

White solid, yield: 43%; Mp: 133–134 °C. ^{1}H NMR (400 MHz, DMSO-d_6) δ 7.86–7.81 (m, 2H), 7.30–7.25 (m, 2H), 5.82–5.78 (m, 2H), 5.37 (s, 1H), 4.88 (d, J = 12.4 Hz, 1H), 4.46 (d, J = 12.7 Hz, 1H), 4.36 (d, J = 4.1 Hz, 1H), 4.32 (d, J = 2.0 Hz, 1H), 4.07 (d, J = 4.6 Hz, 1H), 3.11–3.06 (m, 1H), 2.59 (dt, J = 13.8, 4.1 Hz, 1H), 2.10 (s, 3H), 1.99–1.85 (m, 2H), 1.73 (q, J = 12.7 Hz, 1H), 1.60 (d, J = 15.8 Hz, 2H), 1.44 (q, J = 10.5 Hz, 3H), 1.24–1.15 (m, 1H), 1.08 (dd, J = 12.7, 1.9 Hz, 1H), 0.97–0.91 (m, 1H), 0.89 (s, 3H), 0.87 (s, 4H). ^{13}C NMR (100 MHz, DMSO-d_6) δ 204.1, 170.2, 165.0, 163.4, 148.2, 132.0, 131.9, 127.5, 115.4, 115.1, 112.8, 77.0, 72.0, 66.0, 62.7, 61.9, 59.1, 52.8, 42.9, 41.1, 40.6, 38.9, 33.7, 32.9, 32.5, 27.8, 22.1, 20.7, 17.7. HR-MS(ESI): Calculated for $C_{29}H_{35}FNaO_7$ $[M+Na]^+$: 537.2265, found 537.2250.

Table 2
Changes in relevant biochemical indicators.

Related parameters	NC	20 mg/kg/d	40 mg/kg/d
WBC(× 10^9 L)	4.42 ± 0.79	5.02 ± 1.45	4.21 ± 0.49
RBC(× 10^9 L)	9.75 ± 0.19	9.47 ± 0.1	9.28 ± 0.22
HGB(g/L)	153.20 ± 3.87	147.00 ± 0.89	144.40 ± 1.62
HCT (%)	49.08 ± 1.56	46.67 ± 0.55	46.26 ± 1.29
MCV(fL)	49.90 ± 0.37	49.50 ± 0.57	49.36 ± 0.72
RDW (%)	14.18 ± 0.26	14.32 ± 0.31	14.73 ± 0.44
PLT(× 10^9 L)	788.60 ± 71.35	754.80 ± 150.29	832.80 ± 41.4

4.2.20. (4aR,6R,6aR,9S,11S,11bS,12R,14R)-11b-(acetoxymethyl)-6,11-dihydroxy-4,4-dimeth-yl-8-methylene-7-oxotetradecahydro-6a,9-methanocyclohepta[a]naph-thalen-12-yl-4-chlorobenzoate. (compound 2t)

White solid, yield: 46%; Mp: 135–136 °C. ^{1}H NMR (400 MHz, DMSO-d_6) δ 7.78 (d, J = 2.1 Hz, 1H), 7.77 (d, J = 2.0 Hz, 1H), 7.53 (d, J = 2.0 Hz, 1H), 7.51 (d, J = 2.0 Hz, 1H), 5.81 (d, J = 4.5 Hz, 2H), 5.37 (s, 1H), 4.88 (d, J = 12.4 Hz, 1H), 4.46 (d, J = 12.5 Hz, 1H), 4.36 (d, J = 4.3 Hz, 1H), 4.32 (d, J = 2.1 Hz, 1H), 3.11–3.07 (m, 1H), 2.59 (dt, J = 14.2, 4.1 Hz, 1H), 2.10 (s, 3H), 1.98–1.88 (m, 2H), 1.79–1.56 (m, 4H), 1.54–1.36 (m, 4H), 1.11–1.05 (m, 1H), 0.97–0.91 (m, 1H), 0.89 (s, 3H), 0.87 (s, 4H). ^{13}C NMR (100 MHz, DMSO-d_6) δ 204.0, 170.2, 165.1, 148.1, 137.4, 131.0 (× 2), 129.7, 128.4 (× 2), 112.9, 77.2, 72.0, 66.0, 62.7, 61.9, 59.1, 52.8, 42.8, 41.1, 40.6, 38.9, 33.7, 32.9, 32.5, 27.8, 22.1, 20.7, 17.7. HR-MS(ESI): Calculated for $C_{29}H_{35}ClNaO_7$ $[M+Na]^+$: 553.1969, found 553.2048.

4.2.21. (4aR,6R,6aR,9S,11S,11bS,12R,14R)-11b-(acetoxymethyl)-6,11-dihydroxy-4,4-dimethyl-8-methylene-7-oxotetradecahydro-6a,9-methanocyclohepta[a]naph-thalen-12-yl-4-bromobenzoate. (compound 2u)

White solid, yield: 61%; Mp: 131–133 °C. ^{1}H NMR (400 MHz, DMSO-d_6) δ 7.72–7.65 (m, 4H), 5.80 (d, J = 6.5 Hz, 2H), 5.38 (s, 1H), 4.88 (d, J = 12.4 Hz, 1H), 4.46 (d, J = 12.4 Hz, 1H), 4.37 (d, J = 4.1 Hz, 1H), 4.33 (d, J = 2.1 Hz, 1H), 3.10 (d, J = 3.8 Hz, 1H), 2.59 (dt, J = 13.9, 4.0 Hz, 1H), 2.10 (s, 3H), 1.98–1.86 (m, 2H), 1.73 (q, J = 12.6 Hz, 1H), 1.60 (d, J = 15.6 Hz, 3H), 1.53–1.35 (m, 4H), 1.08 (dd, J = 12.7, 2.2 Hz, 1H), 0.94 (dd, J = 13.0, 4.3 Hz, 1H), 0.89 (s, 3H), 0.87 (s, 4H). ^{13}C NMR (100 MHz, DMSO-d_6) δ 204.0, 170.2, 165.3, 148.1, 131.3 (× 2), 131.2 (× 2), 130.1, 126.5, 112.9, 77.2, 72.00, 66.0, 62.7, 61.9, 59.1, 52.8, 42.8, 41.1, 40.6, 38.9, 33.7, 32.8, 32.5, 27.8, 22.1, 20.7, 17.7. HR-MS(ESI): Calculated for $C_{29}H_{35}BrNaO_7$ $[M+Na]^+$: 597.1464, found 597.1459.

4.2.22. (4aR,6R,6aR,9S,11S,11bS,12R,14R)-11b-(acetoxymethyl)-6,11-dihydroxy-4,4-dimeth-yl-8-methylene-7-oxotetradecahydro-6a,9-methanocyclohepta[a]naph-thalen-12-yl-4-methoxybenzoate. (compound 2v)

White solid, yield: 47%; Mp: 122–123 °C. ^{1}H NMR (400 MHz, DMSO-d_6) δ 7.77–7.71 (m, 2H), 6.99–6.94 (m, 2H), 5.78 (d, J = 10.5 Hz, 2H), 5.36 (s, 1H), 4.88 (d, J = 12.4 Hz, 1H), 4.47 (d,

J = 12.2 Hz, 1H), 4.31 (d, J = 2.0 Hz, 1H), 4.27 (d, J = 4.3 Hz, 1H), 3.79 (s, 3H), 3.06 (d, J = 3.6 Hz, 1H), 2.59 (dt, J = 14.2, 4.2 Hz, 1H), 2.10 (s, 3H), 2.00−1.87 (m, 2H), 1.74 (q, J = 12.4 Hz, 1H), 1.60 (d, J = 17.4 Hz, 3H), 1.53−1.35 (m, 4H), 1.08 (dd, J = 12.7, 2.1 Hz, 1H), 0.96−0.91 (m, 1H), 0.89 (s, 3H), 0.87 (s, 4H). ^{13}C NMR (100 MHz, DMSO-d_6) δ 203.1, 169.1, 164.4, 161.4, 147.3, 130.1 (× 2), 122.1, 112.3 (× 2), 111.5, 75.4, 70.9, 64.9, 61.6, 60.8, 58.0, 54.2, 51.8, 41.9, 40.0, 39.5, 37.8, 32.63, 31.80, 31.39, 26.82, 21.09, 19.65, 16.62. HR-MS(ESI): Calculated for $C_{30}H_{38}NaO_8$ [M+Na]$^+$: 549.2464, found 549.2465.

4.2.23. (4aR,6R,6aR,9S,11S,11bS,12R,14R)-11b-(acetoxymethyl)-6,11-dihydroxy-4,4-dimeth-yl-8-methylene-7-oxotetradecahydro-6a,9-methanocyclohepta[a]naph-thalen-12-yl-4-methylbenzoate. (compound 2w)

White solid, yield: 63%; Mp: 142−143 °C. ^{1}H NMR (400 MHz, DMSO-d_6) δ 7.70−7.66 (m, 2H), 7.23 (d, J = 8.3 Hz, 2H), 5.79 (d, J = 6.7 Hz, 2H), 5.37 (s, 1H), 4.88 (d, J = 12.5 Hz, 1H), 4.47 (d, J = 12.7 Hz, 1H), 4.31 (d, J = 2.0 Hz, 1H), 4.28 (d, J = 4.4 Hz, 1H), 3.07 (d, J = 3.6 Hz, 1H), 2.59 (dt, J = 13.8, 4.1 Hz, 1H), 2.33 (s, 3H), 2.10 (s, 3H), 1.98−1.85 (m, 2H), 1.75 (q, J = 12.6 Hz, 1H), 1.60 (d, J = 15.8 Hz, 3H), 1.54−1.34 (m, 4H), 1.08 (dd, J = 12.8, 2.0 Hz, 1H), 0.96−0.91 (m, 1H), 0.89 (s, 3H), 0.87 (s, 4H). ^{13}C NMR (100 MHz, DMSO-d_6) δ 204.2, 170.2, 165.9, 148.3, 142.6, 129.3 (× 2), 128.71 (× 2), 128.2, 112.7, 76.7, 72.0, 66.0, 62.8, 61.9, 59.1, 52.9, 42.9, 41.1, 40.6, 38.9, 33.7, 32.9, 32.5, 27.9, 22.2, 21.0, 20.7, 17.7. HR-MS(ESI): Calculated for $C_{30}H_{38}NaO_7$ [M+Na]$^+$: 533.2515, found 533.2516.

4.2.24. (4aR,6R,6aR,9S,11S,11bS,12R,14R)-11b-(acetoxymethyl)-6,11-dihydroxy-4,4-dimeth-yl-8-methylene-7-oxotetradecahydro-6a,9-methanocyclohepta[a]naph-thalen-12-yl-4-(trifluoromethyl) benzoate. (compound 2x)

White solid, yield: 43%; Mp: 155−157 °C. ^{1}H NMnR (400 MHz, DMSO-d_6) δ 7.97 (d, J = 8.2 Hz, 2H), 7.84 (d, J = 8.4 Hz, 2H), 5.84 (d, J = 4.8 Hz, 2H), 5.39 (s, 1H), 4.89 (d, J = 12.3 Hz, 1H), 4.48 (d, J = 12.4 Hz, 1H), 4.42 (d, J = 4.4 Hz, 1H), 4.34 (s, 1H), 3.12 (s, 1H), 2.61 (dd, J = 14.0, 4.9 Hz, 1H), 2.11 (s, 3H), 1.99−1.87 (m, 2H), 1.75 (q, J = 12.4 Hz, 1H), 1.62 (d, J = 14.2 Hz, 2H), 1.44 (q, J = 16.2, 14.1 Hz, 4H), 1.20 (dt, J = 14.3, 7.2 Hz, 1H), 1.09 (d, J = 12.3 Hz, 1H), 0.95 (d, J = 11.0 Hz, 1H), 0.89 (s, 3H), 0.88 (s, 4H). ^{13}C NMR (100 MHz, DMSO-d_6) δ 203.9, 170.2, 165.0, 148.1, 134.6, 132.0, 130.0 (× 2), 125.3, 125.1, 122.3, 113.0, 77.5, 72.0, 66.1, 62.7, 61.9, 59.1, 52.8, 42.8, 41.1, 40.6, 38.9, 33.7, 32.8, 32.4, 27.8, 22.1, 20.7, 17.7. HR-MS(ESI): Calculated for $C_{30}H_{35}F_3NaO_7$ [M+Na]$^+$: 587.2233, found 587.2205.

4.2.25. (4aR,6R,6aR,9S,11S,11bS,12R,14R)-11b-(acetoxymethyl)-6,11-dihydroxy-4,4-dimeth-yl-8-methylene-7-oxotetradecahydro-6a,9-methanocyclohepta[a]naph-thalen-12-yl-4-(chloromethyl) benzoate. (compound 2y)

White solid, yield: 56%; Mp: 132−133 °C. ^{1}H NMR (400 MHz, DMSO-d_6) δ 7.71 (d, J = 8.0 Hz, 2H), 7.43 (d, J = 8.3 Hz, 2H), 5.76−5.72 (m, 2H), 5.30 (s, 1H), 4.82 (d, J = 12.5 Hz, 1H), 4.71 (s, 2H), 4.40 (d, J = 12.4 Hz, 1H), 4.29−4.23 (m, 2H), 3.02 (d, J = 3.8 Hz, 1H), 2.53 (dt, J = 14.1, 4.1 Hz, 1H), 2.03 (s, 3H), 1.95−1.81 (m, 3H), 1.54 (d, J = 14.7 Hz, 3H), 1.47−1.30 (m, 4H), 1.04−0.99 (m, 1H), 0.87 (dd, J = 13.1, 4.6 Hz, 1H), 0.82 (s, 3H), 0.81 (s, 4H). ^{13}C NMR (100 MHz, DMSO-d_6) δ 204.1, 170.2, 165.6, 148.2, 142.0, 130.7 (× 2), 129.5 (× 2), 128.5, 112.8, 77.0, 72.0, 66.0, 62.7, 61.9, 59.1, 52.9, 45.3, 42.9, 41.1, 40.6, 38.9, 33.7, 32.9, 32.5, 27.9, 22.2, 20.7, 17.7. HR-MS(ESI): Calculated for$C_{30}H_{37}ClNaO_7$ [M+Na]$^+$: 567.2126, found 567.2149.

4.2.26. (4aR,6R,6aR,9S,11S,11bS,12R,14R)-11b-(acetoxymethyl)-6,11-dihydroxy-4,4-dimethyl-8-methylene-7-oxotetradecahydro-6a,9-methanocyclohepta[a]naph-thalen-12-yl 4-(bromomethyl) benzoate. (compound 2z)

White solid, yield: 43%; Mp: 111−112 °C. ^{1}H NMR (400 MHz, DMSO-d_6) δ 7.78 (d, J = 8.2 Hz, 2H), 7.49 (d, J = 8.3 Hz, 2H), 5.81 (s, 2H), 5.37 (s, 1H), 4.88 (d, J = 12.4 Hz, 1H), 4.78 (s, 2H), 4.47 (d, J = 12.4 Hz, 1H), 4.33 (d, J = 7.0 Hz, 2H), 3.08 (d, J = 3.9 Hz, 1H), 2.60 (dt, J = 14.1, 4.1 Hz, 1H), 2.10 (s, 3H), 1.98−1.86 (m, 2H), 1.80−1.54 (m, 4H), 1.53−1.30 (m, 4H), 1.08 (d, J = 11.9 Hz, 1H), 0.94 (dd, J = 13.4, 3.8 Hz, 1H), 0.89 (s, 3H), 0.87 (s, 4H). ^{13}C NMR (100 MHz, DMSO-d_6) δ 204.1, 170.2, 165.6, 148.2, 142.0, 130.7, 129.5 (× 2), 128.5 (× 2), 112.8, 77.0, 72.0, 66.0, 62.7, 61.9, 59.1, 52.9, 45.3, 42.9, 41.1, 40.6, 38.9, 33.7, 32.9, 32.5, 27.9, 22.2, 20.7, 17.7. HR-MS(ESI): Calculated for $C_{30}H_{37}BrNaO_7$ [M+Na]$^+$: 611.1620, found 611.1719.

4.3. Cell culture

Human oesophageal cancer cells EC109, TE-1, human breast cancer cells MCF-7, human gastric cancer cells MGC-803, human gastric epithelial cell line GES-1, human umbilical vein endothelial cells, the above cells were purchased from China Center for Type Collection (CCTCC, China) and grown in RPMI-1640 medium (Corning, USA) with 10% fetal bovine serum (FBS) (ZETA, USA). Cells were cultured in a humid atmosphere of 5% CO_2 and 95% air at 37 °C.

4.4. Determination of anticancer activity in vitro

All cell viability tests were performed by the SRB method. When the cells were in the logarithmic growth phase, and the cell fusion degree was about 90%, the cells were digested by trypsin and centrifuged to collect the cells. Cell counting plates were used and then evenly seeded in 96-well plates. When the cells begin to divide logarithmically, discard the old medium, and add the medicated medium. At the end of incubation time, the medium was abandoned, and then 100 L 10% TCA solution was added to each well. The plate was incubated in a 4 °C refrigerator in the dark to fix the bottom cells. After 1 h, remove the culture plate, remove the TCA solution, and carefully clean the 96-well plate with pure water to remove excess TCA fixative solution. After washing, put it in the ventilation place for drying. After drying, use the prepared SRB staining solution for cell staining and shaker staining 30 min. And then, 96-well plates were washed five times with pure water containing 1% acetic acid to remove excess dyes. Dried in the ventilated place, then added Tris-HCl (PH10.5), dissolved dyes on the shaker, and detected the absorbance value (OD value) at 560 nM using a microplate reader.

4.5. Colony formation assay

Firstly, EC 109 digestion treatment, which was in the logarithmic growth phase and had a fusion degree of 90%, was used to collect cells. Cells were seeded into 6-well plates according to 1.5×10^3 per well. After waiting for cells to adhere, the medium containing drugs was replaced, and then the medium without drugs was replaced for 24 h in a 5% CO_2 incubator at 37 °C. After replacing the medium, the cells were cultured in a 5% CO_2 incubator at 37 °C for seven days. The cells were observed under a microscope to form a cell colony. Then discard the culture medium and use the 4% paraformaldehyde solution to fix the cells. Add paraformaldehyde and wait 30 min to complete the fixation, discard the fixative, add PBS to wash the fixative on the shaker, wash three times in 5 min each time. After cleaning, 6-well plates were dried and stained with 1 mL crystal violet staining solution for 30 min. After dyeing, the crystal violet dye solution was discarded, and the excess crystal violet dye solution was washed with PBS and dried. After drying, photographs were taken with a camera, and finally, the number of cell clones was analyzed using ImageJ.

4.6. Flow cytomety measure for cells apoptosis

The apoptosis ratio was used by the kit (KeyGEN BioTECH, China) to detect. Cells were evenly put in 6-well plates, and 6 * 10^4 cells were incubated in each well. When cells adhered to each other and began to grow logarithmically, the old medium was discarded, and the medium containing drugs was added to the incubator for 24 h. After waiting for 24 h, the 6-well plate was digested with trypsin without EDTA, and the cells were collected. During the treatment, the cells were treated gently to avoid damage to the cells. Use EP tubes to collected the cell, and 500 L of Binding Buffer was added to each tube to resuspend the cells. Then 5 L of Annexin V-FITC staining solution and 5 L of PI staining solution were added respectively, mixed evenly and stained for 15 min in the dark at room temperature. And then use the flow cytometry to test the apoptosis ratio (BD Bioscience, USA).

4.7. Detection of cell mitochondrial membrane potential

The change of mitochondrial membrane potential after compound treatment was detected using a kit (KeyGEN BioTECH, China). The cell inoculation procedure was the same as 4.10. After 24 h of drug treatment, the cells were collected into EP tubes. Samples were stained with JC-1 staining solution. Flow cytometry was used for detection.

4.8. Measurement of intracellular ROS generation

Cellular reactive oxygen species were detected by flow cytometry using a kit. The method of cell incubation and drug addition was the same as that of 4.10. After collecting the cells, the staining solution was added and incubated in a cell incubator at 37 C for 20 min. Finally, the reactive oxygen species in the samples were detected by flow cytometry.

4.9. Western blot analysis

Western Blotting was used to detect protein changes in compound-treated cell samples. First, the cells were cultured to the appropriate state and then added drugs. The cells were cultured in the incubator for 24 h after drug addition and digested with trypsin. Add the RIPA lysis solution, which can crack the cell. Then use a centrifuge to centrifuge the sample. The supernatant was collected, and then the protein concentration was detected by the BCA method. Add the appropriate Loading Buffer to the sample. The protein was further denatured using boiling water. The experiments were then carried out using SDS-PAGE, and finally, the glue was transferred to the PVDF membrane (General Electric Company, USA). Use 5% skimmed milk for closure. When blank is over, incubation is performed with an antibody (Bcl-2, Bax, Bim, Cyto C, Bad, Cleaved-Caspase 9, Cleaved-Caspase 7, Cleaved-Caspase 3, Cleaved PARP, p-JNK, p-MKK4, p-ASK1, p-CJUN, β-actin (1000 × dilution)). And then the immunoblots were visualized by enhanced chemiluminescence kit (Thermo Fish, USA).

4.10. Tumour transplantation in nude mice

Twenty-four female BALB/c nude mice were purchased, and the nude mice were housed in an SPF-grade animal room, with five per cage. When the nude mice adapt in the environment for five days, EC109 cells that had been cultured and in good condition were collected and counted. After counting, use the PBS to levitate the cell. Underarm injection for nude mice and each mouse was inoculated with 1.5×10^6 EC109 cells. After the injection, the animals' body weight and tumour tissue size were measured. When the average tumour volume reached 100 mm^3, the animals were divided into three groups, and the administration was started the next day. In the NC group, 200 μL of physiological saline was injected intraperitoneally. The low dose of Compound **2y** was 20 mg/kg/day, and the high dose was 40 mg/kg/day. Nude mice were weighed once a day during dosing, and the tumour volume was measured. Nude mice were sacrificed 14 days after the administration, and nude mice were dissected and weighed and photographed for recording.

4.11. HE staining experiment

Nude mouse xenografts and main organs were fixed in paraformaldehyde for one week and then embedded in paraffin. Cut paraffin blocks into 5 μm sections. The Leica (Leica, Germany) fully automatic HE dyeing machine is used for dewaxing, dyeing, dehydration, and other steps. Leica DM 300 microscope is used to get the picture from slices.

4.12. Tissue protein extraction and tissue protein western blotting

The tumour tissue was disrupted using abrasion. Slowly add liquid nitrogen during the grinding process to cool down until the tissue ends in debris. The remaining steps are similar to Western Blotting experiments at the cellular level.

4.13. Hematological index in nude mice

Use the curved forceps to remove the eyeball of the nude mouse and collect the blood into the blood collection tube. Press the heart of the nude mouse to make the blood flow out quickly. The heart should be pressed lightly to prevent nude mice from dying during blood collection. Centrifuge the sample using a centrifuge and take the serum into a new EP tube. The kit (JianCheng, China) was used to detect various hematological indexes of nude mice. Follow the kit instructions.

4.14. Statistical analysis

All data are expressed as "mean ± SD". GraphPad Prism 8.0 was used for statistical analysis. Nude mouse xenograft experiments were performed using the *t*-test, $P < 0.05$ considered statistically significant. Western blotting experiments were performed by one-way analysis of variance. $P < 0.05$ considered the data to be statistically different.

Declaration of competing interest

The authors declare that they have no known competing financial interests or personal relationships that could have appeared to influence the work reported in this paper.

Acknowledgement

This work was supported by grants from the National Natural Science Foundation of China (No. U1904156, No. U1904163), and Zhengzhou University Student Innovation Experiment Project (UIEP).

Appendix A. Supplementary data

Supplementary data to this article can be found online at https://doi.org/10.1016/j.ejmech.2020.112789.

References

[1] A. Rejhova, A. Opattova, A. Cumova, D. Sliva, P. Vodicka, Natural compounds and combination therapy in colorectal cancer treatment, Eur. J. Med. Chem. 144 (2018) 582–594.

[2] P.B. Goncalves, N.C. Romeiro, Multi-target natural products as alternatives against oxidative stress in chronic obstructive pulmonary disease (COPD), eur, J. Med. Chem. 163 (2019) 911–931.

[3] R.A. Otvos, K.B.M. Still, G.W. Somsen, A.B. Smit, J. Kool, Drug discovery on natural products: from ion channels to nAChRs, from nature to libraries, from analytics to assays, SLAS discovery : advancing life sciences R & D 24 (2019) 362–385.

[4] M. Liu, W. Wang, H. Sun, J. Pu, Diterpenoids from Isodon species: an update, Nat. Prod.t Rep 34 (2017) 1090–1140.

[5] A. Ohsaki, M. Ozawa, K. Komiyama, A. Kishida, T. Isobe, The cytotoxic activity of diterpenoids from Isodon species, Nat. Prod. Commun 7 (2012) 977.

[6] X. Liu, J. Yang, W.G. Wang, Y. Li, J.Z. Wu, J.X. Pu, H.D. Sun, Diterpene alkaloids with an aza-ent-kaurane skeleton from Isodon rubescens, J. Nat. Prod. 78 (2015) 196–201.

[7] M.T. Islam, Diterpenes and their derivatives as potential anticancer agents, Phytother Res. : PT 31 (2017) 691–712.

[8] H.D. Sun, S.X. Huang, Q.B. Han, Diterpenoids from Isodon species and their biological activities, Nat. Prod.t Rep 23 (2006) 673–698.

[9] C. Ding, Y. Zhang, H. Chen, Z. Yang, C. Wild, L. Chu, H. Liu, Q. Shen, J. Zhou, Novel nitrogen-enriched oridonin analogues with thiazole-fused A-ring: protecting group-free synthesis, enhanced anticancer profile, and improved aqueous solubility, J. Med. Chem. 56 (2013) 5048–5058.

[10] Y. Ding, C. Ding, N. Ye, Z. Liu, E.A. Wold, H. Chen, C. Wild, Q. Shen, J. Zhou, Discovery and development of natural product oridonin-inspired anticancer agents, Eur. J. Med. Chem. 122 (2016) 102–117.

[11] D. Li, T. Han, S. Xu, T. Zhou, K. Tian, X. Hu, K. Cheng, Z. Li, H. Hua, J. Xu, Antitumor and antibacterial derivatives of oridonin: a main composition of dong-ling-cao, Molecules 21 (2016) 575.

[12] H. Li, J. Mu, J. Sun, S. Xu, W. Liu, F. Xu, Z. Li, J. Xu, H. Hua, D. Li, Hydrogen sulfide releasing oridonin derivatives induce apoptosis through extrinsic and intrinsic pathways, Eur. J. Med. Chem. 187 (2020) 111978.

[13] S. Xu, L. Pei, C. Wang, Y.K. Zhang, D. Li, H. Yao, X. Wu, Z.S. Chen, Y. Sun, J. Xu, Novel Hybrids of Natural Oridonin-Bearing Nitrogen Mustards as Potential Anticancer Drug Candidates, vol. 5, ACS. Med. Chem. Lett, 2014, pp. 797–802.

[14] S. Xu, H. Yao, S. Luo, Y.K. Zhang, D.H. Yang, D. Li, G. Wang, M. Hu, Y. Qiu, X. Wu, H. Yao, W. Xie, Z.S. Chen, J. Xu, A novel potent anticancer compound optimized from a natural oridonin scaffold induces apoptosis and cell cycle arrest through the mitochondrial pathway, J. Med. Chem. 60 (2017) 1449–1468.

[15] H. Yang, J. Huang, Y. Gao, Z. Wen, L. Peng, X. Ci, Oridonin attenuates carrageenan-induced pleurisy via activation of the KEAP-1/Nrf2 pathway and inhibition of the TXNIP/NLRP3 and NF-kappaB pathway in mice, Inflammopharmacology 28 (2020) 513–523.

[16] Y.C. Yang, C.S. Wang, M.C. Wei, A green approach for the extraction and characterization of oridonin and ursolic and oleanolic acids from Rabdosia rubescens and its kinetic behavior, Food Chem. 319 (2020) 126582.

[17] Y.J. Liao, H.Y. Bai, Z.H. Li, J. Zou, J.W. Chen, F. Zheng, J.X. Zhang, S.J. Mai, M.S. Zeng, H.D. Sun, J.X. Pu, D. Xie, Longikaurin A, a natural ent-kaurane, induces G2/M phase arrest via downregulation of Skp2 and apoptosis induction through ROS/JNK/c-Jun pathway in hepatocellular carcinoma cells, Cell Death Dis. 5 (2014) e1137.

[18] Y. Ke, W. Wang, L.F. Zhao, J.J. Liang, Y. Liu, X. Zhang, K. Feng, H.M. Liu, Design, synthesis and biological mechanisms research on 1,2,3-triazole derivatives of Jiyuan Oridonin A, Bioorg. Med. Chem. 26 (2018) 4761–4773.

[19] Y. Ke, J.J. Liang, R.J. Hou, M.M. Li, L.F. Zhao, W. Wang, Y. Liu, H. Xie, R.H. Yang, T.X. Hu, J.Y. Wang, H.M. Liu, Synthesis and biological evaluation of novel Jiyuan Oridonin A-1,2,3-triazole-azole derivatives as antiproliferative agents, Eur. J. Med. Chem. 157 (2018) 1249–1263.

[20] Y. Ma, Y. Ke, X. Zi, W. Zhao, X. Shi, H. Liu, Jaridonin, a novel ent-kaurene diterpenoid from Isodon rubescens, inducing apoptosis via production of reactive oxygen species in esophageal cancer cells, Curr. Cancer Drug Targets 13 (2013) 611–624.

[21] B. de las Heras, S. Hortelano, N. Giron, P. Bermejo, B. Rodriguez, L. Bosca, Kaurane diterpenes protect against apoptosis and inhibition of phagocytosis in activated macrophages, Br. J. Pharmacol. 152 (2007) 249–255.

[22] X. Hu, Z. Bai, J. Qiao, H. Li, S. Xu, X. Wang, Y. Xu, J. Xu, H. Hua, D. Li, Effective enmein-type mimics of clinical candidate HAO472: design, synthesis and biological evaluation, Eur, J. Med. Chem. 171 (2019) 169–179.

[23] J. Neumann, Y. Yang, R. Kohler, M. Giaisi, M. Witzens-Harig, D. Liu, P.H. Krammer, W. Lin, M. Li-Weber, Mangrove dolabrane-type of diterpenes tagalsins suppresses tumor growth via ROS-mediated apoptosis and ATM/ATR-Chk1/Chk2-regulated cell cycle arrest, Int. J. Canc. 137 (2015) 2739–2748.

[24] C. Ding, Y. Zhang, H. Chen, Z. Yang, C. Wild, N. Ye, C.D. Ester, A. Xiong, M.A. White, Q. Shen, Oridonin ring A-based diverse constructions of enone functionality: identification of novel dienone analogues effective for highly aggressive breast cancer by inducing apoptosis, J. Med. Chem. 56 (2013) 8814–8825.

[25] S. Xu, S. Luo, H. Yao, H. Cai, X. Miao, F. Wu, D.H. Yang, X. Wu, W. Xie, H. Yao, Z.S. Chen, J. Xu, Probing the anticancer action of oridonin with fluorescent analogues: visualizing subcellular localization to mitochondria, J. Med. Chem. 59 (2016) 5022–5034.

[26] Y. Xia, C.S. Lam, W. Li, M.S. Sarwar, K. Liu, K.M. Lee, H.J. Zhang, S.W. Tsang, Flexicaulin A, an ent-kaurane diterpenoid, activates p21 and inhibits the proliferation of colorectal carcinoma cells through a non-apoptotic mechanism, Int. J. Mol. Sci. 20 (2019).

[27] L. Guo, S.W. Tsang, T.X. Zhang, K.L. Liu, Y.F. Guan, B. Wang, H.D. Sun, H.J. Zhang, M.S. Wong, Efficient semisynthesis of (-)-Pseudoirroratin A from (-)-Flexicaulin A and assessment of their antitumor activities, ACS Med. Chem. Lett. 8 (2017) 372–376.

[28] Y. Ke, T.X. Hu, J.F. Huo, J.K. Yan, J.Y. Wang, R.H. Yang, H. Xie, Y. Liu, N. Wang, Z.J. Zheng, Y.X. Sun, C. Wang, J. Du, H.M. Liu, Synthesis and in vitro biological evaluation of novel derivatives of Flexicaulin A condensation with amino acid trifluoroacetate, Eur. J. Med. Chem. 182 (2019) 111645.

[29] H.J. Zhang, H.D. Sun, Diterpenoids from rabdosia flexicaulis, Phytochemistry 28 (1989) 3534–3536.

[30] M. Panda, S.K. Tripathi, B.K. Biswal, Plumbagin promotes mitochondrial mediated apoptosis in gefitinib sensitive and resistant A549 lung cancer cell line through enhancing reactive oxygen species generation, Mol. Biol. Rep. 47 (2020) 4155–4168.

[31] P. Oliva, R. Romagnoli, S. Manfredini, A. Brancale, S. Ferla, E. Hamel, R. Ronca, F. Maccarinelli, A. Giacomini, F. Rruga, E. Mariotto, G. Viola, R. Bortolozzi, Design, synthesis, in vitro and in vivo biological evaluation of 2-amino-3-aroylbenzo[b]furan derivatives as highly potent tubulin polymerization inhibitors, Eur. J. Med. Chem. 200 (2020), 112448.

[32] B. Mansoori, A. Mohammadi, S. Shirjang, B. Baradaran, HMGI-C suppressing induces P53/caspase9 axis to regulate apoptosis in breast adenocarcinoma cells, Cell Cycle 15 (2016) 2585–2592.

[33] B.I. Kim, J.H. Kim, D.Y. Sim, M. Nam, J.H. Jung, B. Shim, J. Lee, S.H. Kim, Inhibition of JAK2/STAT3 and activation of caspase9/3 are involved in KYS05090Sinduced apoptosis in ovarian cancer cells, Int. J. Oncol. 55 (2019) 203–210.

[34] R. Florent, L.B. Weiswald, B. Lambert, E. Brotin, E. Abeilard, M.H. Louis, G. Babin, L. Poulain, M. N'Diaye, Bim, Puma and Noxa upregulation by Naftopidil sensitizes ovarian cancer to the BH3-mimetic ABT-737 and the MEK inhibitor Trametinib, Cell Death Dis. 11 (2020) 380.

[35] S. Laszig, C. Boedicker, T. Weiser, S. Knapp, S. Fulda, The novel dual BET/HDAC inhibitor TW09 mediates cell death by mitochondrial apoptosis in rhabdomyosarcoma cells, Canc. Lett. 486 (2020) 46–57.

[36] W. Zhang, H. Xiong, J. Pang, Z. Su, L. Lai, H. Lin, B. Jian, W. He, H. Yang, Y. Zheng, Nrf2 activation protects auditory hair cells from cisplatin-induced ototoxicity independent on mitochondrial ROS production, Toxicol. Lett. 331 (2020) 1–10.

[37] A. Nasimian, P. Farzaneh, F. Tamanoi, S.Z. Bathaie, Cytosolic and mitochondrial ROS production resulted in apoptosis induction in breast cancer cells treated with Crocin: the role of FOXO3a, PTEN and AKT signaling, Biochem. Pharmacol. 177 (2020), 113999.

[38] J. Yuan, Y. Lu, H. Wang, Y. Feng, S. Jiang, X.H. Gao, R. Qi, Y. Wu, H.D. Chen, Paeoniflorin resists H2O2-induced oxidative stress in melanocytes by JNK/Nrf2/HO-1 pathway, Front. Pharmacol. 11 (2020) 536.

[39] Y. Ding, Q. Xie, W. Liu, Z. Pan, X. Fan, X. Chen, M. Li, W. Zhao, D. Li, Q. Zheng, Neochamaejasmin A induces mitochondrial-mediated apoptosis in human hepatoma cells via ROS-dependent activation of the ERK1/2/JNK signaling pathway, Oxid Med Cell Longev 2020 (2020), 3237150.

[40] Y. Li, H. Ding, L. Liu, Y. Song, X. Du, S. Feng, X. Wang, X. Li, Z. Wang, X. Li, J. Li, J. Wu, G. Liu, Non-esterified fatty acid induce dairy cow hepatocytes apoptosis via the mitochondria-mediated ROS-JNK/ERK signaling pathway, Front Cell Dev Biol 8 (2020) 245.

[41] D.M. Hanafy, P.D. Prenzler, G.E. Burrows, S. Gurusinghe, B.M. Thejer, H.K. Obied, R.A. Hill, Neuroprotective activity of mentha species on hydrogen peroxide-induced apoptosis in SH-SY5Y cells, Nutrients 12 (2020).

[42] C.M. Pilato, J.H. Park, L. Kong, C. d' Ydewalle, D. Valdivia, K.S. Chen, I. Griswold-Prenner, C.J. Sumner, Motor neuron loss in SMA is not associated with somal stress-activated JNK/c-Jun signaling, Hum. Mol. Genet. 28 (2019) 3282–3292.

[43] H. Weng, H. Huang, B. Dong, P. Zhao, H. Zhou, L. Qu, Inhibition of miR-17 and miR-20a by oridonin triggers apoptosis and reverses chemoresistance by derepressing BIM-S, Canc. Res. 74 (2014) 4409–4419.

[44] R. Chirillo, I. Aversa, A. Di Vito, A. Salatino, A.M. Battaglia, A. Sacco, M.A. Di Sanzo, M.C. Faniello, B. Quaresima, C. Palmieri, F. Biamonte, F. Costanzo, FtH-mediated ROS dysregulation promotes CXCL12/CXCR4 Axis Activation and EMT-like trans-differentiation in erythroleukemia K562 cells, Front Oncol 10 (2020) 698.

[45] D.F. Meng, L.L. Guo, L.X. Peng, L.S. Zheng, P. Xie, Y. Mei, C.Z. Li, X.S. Peng, Y.H. Lang, Z.J. Liu, M.D. Wang, D.H. Xie, D.T. Shu, H. Hu, S.T. Lin, H.F. Li, F.F. Luo, R. Sun, B.J. Huang, C.N. Qian, Antioxidants suppress radiation-induced apoptosis via inhibiting MAPK pathway in nasopharyngeal carcinoma cells, Biochem. Biophys. Res. Commun. 527 (2020) 770–777.

[46] M. Jalili-Nik, M.M. Sadeghi, E. Mohtashami, H. Mollazadeh, A.R. Afshari, A. Sahebkar, Zerumbone promotes cytotoxicity in human malignant glioblastoma cells through reactive oxygen species (ROS) generation, Oxid Med Cell Longev 2020 (2020), 3237983.